Journal of Advanced Ceramics
2022, **11**(6): 835–861
https://doi.org/10.1007/s40145-022-0580-8
ISSN 2226-4108
CN 10-1154/TQ

Review

Advanced inorganic/polymer hybrid electrolytes for all-solid-state lithium batteries

Xiaoyu JI[a,b,†], Yiruo ZHANG[b,†], Mengxue CAO[c], Quanchao GU[a], Honglei WANG[a], Jinshan YU[a], Zi-Hao GUO[b,*], Xingui ZHOU[a,*]

[a]*Science and Technology on Advanced Ceramic Fibers and Composites Laboratory*, *College of Aerospace Science and Engineering*, *National University of Defense Technology*, *Changsha 410073*, *China*
[b]*South China Advanced Institute for Soft Matter Science and Technology*, *School of Molecular Science and Engineering*, *South China University of Technology*, *Guangzhou 510640*, *China*
[c]*Department of Chemical and Environmental Engineering*, *Yale University*, *New Haven 06511*, *USA*

Received: October 21, 2021; Revised: January 7, 2022; Accepted: February 1, 2022

Abstract: Solid-state batteries have become a frontrunner in humankind's pursuit of safe and stable energy storage systems with high energy and power density. Electrolyte materials, currently, seem to be the Achilles' heel of solid-state batteries due to the slow kinetics and poor interfacial wetting. Combining the merits of solid inorganic electrolytes (SIEs) and solid polymer electrolytes (SPEs), inorganic/polymer hybrid electrolytes (IPHEs) integrate improved ionic conductivity, great interfacial compatibility, wide electrochemical stability window, and high mechanical toughness and flexibility in one material, having become a sought-after pathway to high-performance all-solid-state lithium batteries. Herein, we present a comprehensive overview of recent progress in IPHEs, including the awareness of ion migration fundamentals, advanced architectural design for better electrochemical performance, and a perspective on unconquered challenges and potential research directions. This review is expected to provide a guidance for designing IPHEs for next-generation lithium batteries, with special emphasis on developing high-voltage-tolerance polymer electrolytes to enable higher energy density and three-dimensional (3D) continuous ion transport highways to achieve faster charging and discharging.

Keywords: solid-state electrolytes (SSEs); hybrid electrolytes; energy density; electrical energy storage (EES); lithium batteries

1 Introduction

Unprecedented advances in electrified transportation, grid-scale storage, portable electronics, and intelligent machines are placing insatiable demand for more efficient and powerful electrical energy storage (EES) devices [1–4]. Meanwhile, the safety concerns are not only existing in small and isolated devices, but also in systems with larger scale, multiple components, and much closer to human bodies [3,5]. Although attractive energy density and sustainability of lithium-ion batteries (LIBs) have enabled their huge commercial success as

† Xiaoyu Ji and Yiruo Zhang contributed equally to this work.
* Corresponding authors.
E-mail: Z.-H. Guo, guozihao@scut.edu.cn;
X. Zhou, zhouxinguilmy@163.com

EES devices, the organic liquid electrolytes they contain are unstable and combustible, leading to severe safety hazards that are culpable for many catastrophic battery incidents. Moreover, today's state-of-the-art LIBs present a volumetric energy density up to 770 $W{\cdot}h{\cdot}L^{-1}$, which unfortunately, may reach their ceiling soon [6]. All-solid-state lithium batteries that use solid-state electrolytes (SSEs) to replace the liquid ones have attracted great attention, as potentially safe and stable EES systems with higher energy density and power density (fast discharging/charging performance) [7–9].

Interest in electrochemical cells with SSEs can date back to the 1830s—the discovery of fast ion transport in solid-state PbF_2 and Ag_2S materials by Michael Faraday [10]. Nevertheless, intense exploitation and rapid development of SSEs emerged in the past decades, driven by the renaissance of rechargeable batteries with metallic lithium (Li) anodes. Such anodes offer the highest anode capacity, lowest electrochemical potential, and allow the use of lightweight sulfur (S) or air cathodes to achieve higher energy density [9], but suffer from uneven Li electrodeposition and uncontrolled dendrite growth, especially in cells based on organic liquid electrolytes [11,12]. Solid ionic conductors with superior chemical stability and mechanical rigidity therefore become a pivotal material to satisfy the requirements of these next-generation high-energy lithium batteries [13].

To date, the SSEs can be classified into two major categories: solid inorganic electrolytes (SIEs) and solid polymer electrolytes (SPEs) [13,14]. As depicted in Fig. 1, SIEs exhibit high ionic conductivity (> 10^{-4} $S{\cdot}cm^{-1}$ at room temperature (RT)), broad electrochemical window (> 4.0 V vs. Li/Li^+), superior mechanical strength (> 1 GPa for oxides), and absolute incombustibility. Furthermore, SIEs allow the transfer of lithium cations (Li^+) only, avoiding the ionic concentration polarization that limits the cell current and thus enabling higher current densities and quicker charging time. Unfortunately, these inorganic materials are brittle and show poor contact with electrodes, leading to large interfacial impedance and sacrificed cycle stability [15,16]. In this respect, flexible SPEs seem to be a natural alternative as they exhibit better interfacial wetting, and can compensate the electrode volume changes through their elastic and plastic deformation [17–19]. However, the ionic conductivity of SPEs (< 10^{-5} $S{\cdot}cm^{-1}$) is too low for RT battery applications. Even at elevated temperatures above 80 ℃, their rate capabilities still underperform [20]. Although numerous interfacial and molecular engineering strategies have been developed to tackle the above issues [21,22], challenges still remain for any single SSE to meet all the requirements for high-performance Li batteries.

To integrate the merits of SIEs and SPEs and avert their drawbacks, recently, emerging IPHEs have been intensely studied as a promising candidate for all-solid-state Li batteries. Using both SIE and SPE as the ion transfer media, IPHEs combine their advantages through judicious architectural design. For instance, one of the eminent strategies is via multi-layer architectures,

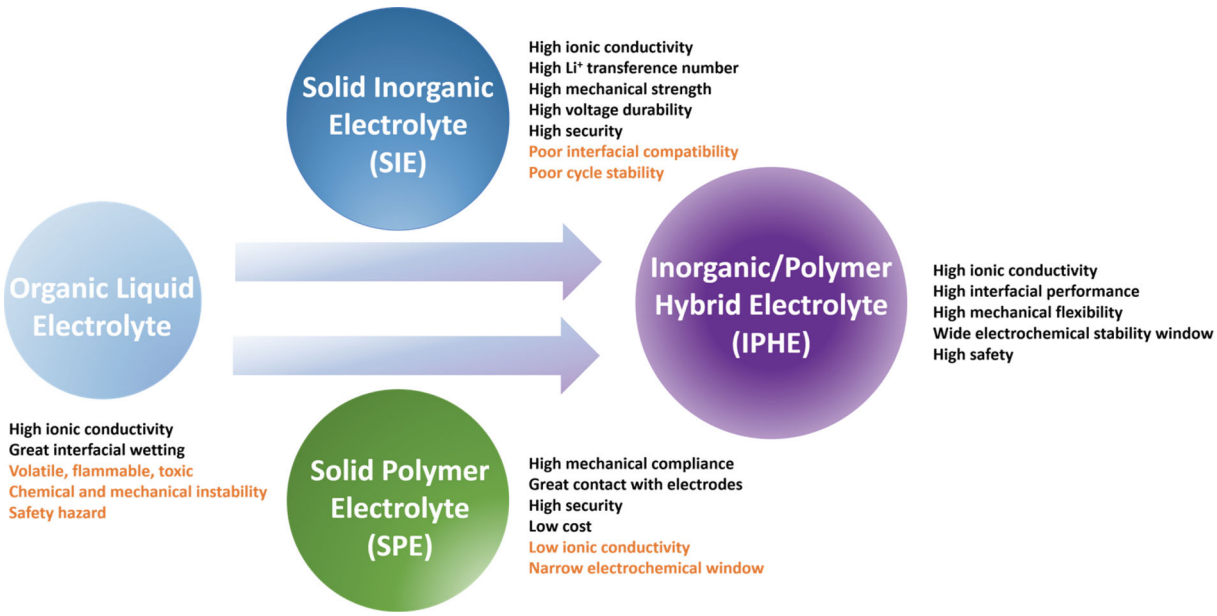

Fig. 1 Evolution of electrolyte materials in lithium batteries from commercial liquid electrolytes to SIE, SPE, and IPHE.

where one or two specific polymer layers locate on one or both sides of the highly conductive SIE layer [23–25]. Another prevailing strategy is based on ceramic/polymer composites with various nanostructures, consisting of flexible SPE matrix and SIE reinforcements such as nanoparticles, nanowires, and three-dimentional (3D) frameworks [26–29]. Given the programmable architectures and distinct ion-conducting behaviors, IPHEs have become a fascinating research topic that has great potential to make breakthroughs in the current battery community.

At present, IPHEs have demonstrated enhanced interfacial performance, ionic conductivity, Li^+ transference number (t^+), electrochemical stability window, and long-term stability [30–32]. Multifarious architectures with varied compositions have been proposed, attracting ongoing attentions. Focusing on these advanced architectures, this review summarizes the recent progress in IPHEs used in all-solid-state Li batteries. Firstly, the ion transport mechanisms in IPHEs and their two primary components are illuminated. On this basis, we systematically survey and discuss the micro/nano structural design of IPHEs, with emphasis on the multi-layer architectures with elegant interfacial properties and the ceramic/polymer composite architectures for efficient ion transport. Finally, a perspective on the unconquered challenges and possible research directions is presented for the future development of IPHEs in electrochemical energy storage and modern battery industry.

2 Mechanism of ion transport in SSEs

The development of high-performance IPHEs depends on a better understanding of their ion-conducting mechanism. Therefore, the fundamentals of ion transport in IPHEs and their two significant components, SIEs and SPEs, are discussed in this section.

2. 1 Ion transport in SIEs

The widely-studied SIEs mainly include LISICON-type $Li_{14}Zn(GeO_4)_4$ [33], NASICON-type $Li_{1+x}Al_xTi_{2-x}(PO_4)_3$ (LATP) and $Li_{1+x}Al_xGe_{2-x}(PO_4)_3$ (LAGP) [34], perovskite-type $Li_{3x}La_{2/3-x}TiO_3$ (LLTO) [35], antiperovskite-type Li_3OCl [36], garnet-type $Li_7La_3Zr_2O_{12}$ (LLZO) [37], sulfide electrolyte family such as $Li_{10}GeP_2S_{12}$ (LGPS) [38], Li_2S–P_2S_5 glass–ceramic electrolyte [39,40], as well as other ceramics [41]. These ceramic Li^+ conductors possess a periodic structure with a spatial arrangement of mobile species and the coordinated polyhedrons. As depicted in Fig. 2(a), the defects within the framework, including Frenkel defects (interstitial ions accompanied with vacancies) and Schottky defects (anion vacancies accompanied with cation vacancies), make the most contribution to the fast ion movement [15,42]. Through Frenkel defects, normally, the interstitial ions diffuse by continuously displacing Li^+ in adjacent sites based on a knock-off mechanism, and Schottky defects can create loads of vacancies available for ion hopping among the lattices. Besides, the ions can also migrate through the distorted lattice near grain boundaries and electrode interfaces, which is induced by the potential difference and mobile carrier redistribution.

The topology of the ceramic framework and concentration of the defects are two principal factors to determine the ion migration ability. Investigations of the Li^+ migration barrier in various anion-host matrices reveal the relationship between anion arrangement and energy landscape for ion transport (Fig. 2(b)) [43]. Compared to fcc and hcp anion lattice, the bcc packed anion matrix allows the direct Li^+ hopping between adjacent tetrahedral sites, therefore offering the lowest activation barrier and highest ionic conductivity. The bcc topology is presented in some highly conductive SIEs, including sulfide LGPS and antiperoskite-type Li_3OCl. In terms of defects, sufficient and interconnected interstices and vacancies are profitable to the fast Li^+ conduction. On one hand, doping aliovalent cations is an effective way to increase the defect and carrier concentration, i.e., the various X–LLZO or LLZXO garnet-type electrolytes (X = doping cations of Ga, Ta, Ca, Al, etc.) [44]. Generally, doping higher-valence cations can create cation vacancy or anion interstitials, whereas doping lower-valence cations can build cation interstitials or anion vacancies [15]. On the other hand, the computational simulation indicates a cooperative ion motion in various well-known fast Li^+ conductors, including LLZO, LATP, and LGPS. Instead of isolated ion hopping (Fig. 2(c)), the concerted migration of multiple ions to the nearest sites has a lower energy barrier, owing to the strong ion–ion interactions and interconnected sites [45].

At present, the state-of-the-art oxide-based and sulfide-based SIEs have achieved the ionic conductivity of 10^{-3}–10^{-2} $S \cdot cm^{-1}$ at RT [46,47], which is comparable to or even exceeds that of liquid electrolyte/separator systems in commercial LIBs. However, the intrinsic brittleness and rigidity of SIEs, especially for oxide

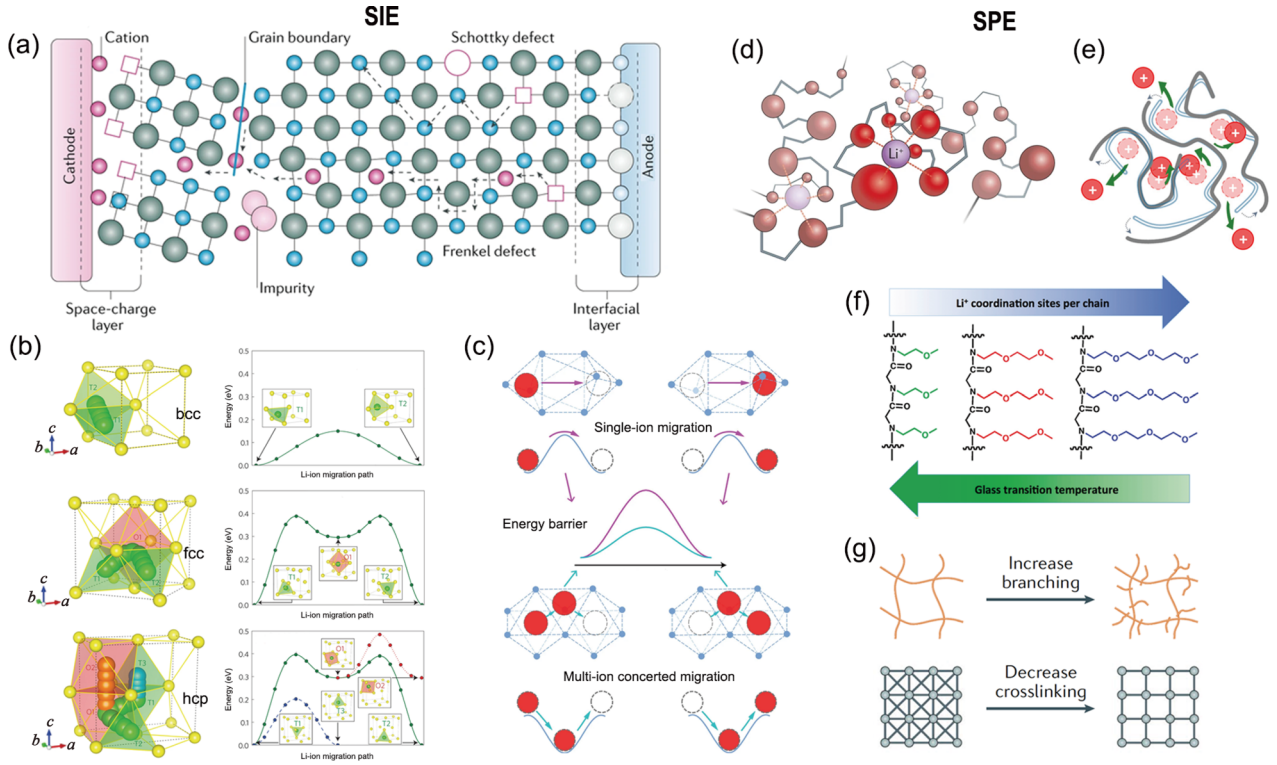

Fig. 2 Ion transport mechanisms in (a–c) SIEs and (d–g) SPEs: (a) schematic showing the Schottky defects, Frenkel defects, free space at grain boundaries, and interfacial layer; (b) ion transport pathways (left panels) and calculated energy landscapes (right panels) in body-centered cubic (bcc), face-centered cubic (fcc), and hexagonal close-packed (hcp) sulphur lattices, where the bcc lattice shows the lowest energy barriers; (c) schematic showing the single-ion migration (the upper inset) versus multi-ion concerted migration (the lower inset) in SIEs; (d) illustration of Li^+ (purple) solvation by oxygen atoms (red) of the poly(ethylene oxide) (PEO) electrolyte; (e) schematic diagram showing the ion transport in SPEs through segmental relaxation and ion hopping; (f, g) schematics showing the molecular engineering methods that reduce the glass transition temperature (T_g) and lead to higher ionic conductivity. Reproduced with permission from Ref. [13] for (a), © Springer Nature Limited 2020; Ref. [43] for (b), © Nature Publishing Group 2015; Ref. [45] for (c), © The Author(s) 2017; Ref. [22] for (d, g), © Springer Nature Limited 2019; Ref. [48] for (e), © American Chemical Society 2020; Ref. [49] for (f), © American Chemical Society 2012.

ceramics, make it hard to buffer the volume change of electrode materials during cycling, leading to a loss of close contact and huge interfacial impedance. Also, their ideal bulk ionic conductivity relies heavily on a dense ceramic structure, translating to severe synthetic temperatures over 1000 ℃. Although sulfides are relatively ductile and exhibit facile processing temperature, they are sensitive to air (generating H_2S gas), and prone to be reduced at Li metal anode and oxidized at the cathodic interface [50–52]. Incorporation with protective or soft layers to stabilize the electrolyte/ electrode interfaces and enhance the interfacial contact is required for SIEs to improve their electrochemical performance.

2. 2 Ionic transport in SPEs

SPEs conduct ions typically through the segmental dynamics of polymer chains. PEO is the firstly discovered polymer that can dissolve Li salts and is still one widely studied and successfully used SPEs at present [53,54]. The ion transport mechanism involves the dissociation of Li salts by polymer chains (Fig. 2(d)) and the transfer of complexed Li^+ via chain segmental dynamics and ion hopping (Fig. 2(e)) [22,45]. Ionic conductivity (σ) is a product of ionic charge (q), concentration of mobile ions (c), and mobility (μ) at which the ions can move through the abovementioned mechanism: $\sigma = qc\mu$ [55]. The high dielectric constant of PEO makes it effectively dissolve Li salts and coordinate with Li cations to achieve a high c. The abundant EO motifs along the backbones provide interconnected donor sites and requisite flexibility for fast ion migration. Beyond PEO, other SPEs include poly(propylene oxide) (PPO), polyacrylonitrile (PAN), polyvinylidene fluoride (PVDF), polymethyl methacrylate (PMMA), poly(vinyl carbonate) (PVC), and so forth [56].

Although specific instances demonstrate ion-conducting

behavior in crystalline domains [57–59], it is widely recognized that ion transport in SPEs occurs in the amorphous phase above T_g and is strongly coupled to their local segmental relaxation. At RT, however, most of the existing SPEs are crystalline or semi-crystalline. Even though some amorphous PEO electrolytes exhibit relatively fast segmental relaxation time (10^{-7}–10^{-6} s) at RT, it is still much slower than the required value (*ca.* 10^{-10} s) to achieve the eligible ionic conductivity for practical battery application [45]. Suppressing crystallinity and lowering the T_g of polymer chains are the major design principles to enhance the segmental motion, and thus increase the ionic conductivity. On this consensus, scalable polymer engineering strategies have been developed including side-chain engineering [46,60,61], crosslinked polymers [62–64], hyperbranched polymers [65], and others [66]. Increasing side chain length from one EO unit to three is verified to enable to reduce the T_g and increase the ionic conductivity tenfold (Fig. 2(f)) [46]. Recent experimental and theoretical studies reveal that the enhanced ionic conductivity with the side chain length is attributed to the increased segmental mobility and effective solvation sites of the longer side chains [67–69]. Increasing the degree of branching and decreasing the degree of crosslinking in crosslinked SPEs are also efficient methods to reduce crystallinity and T_g (Fig. 2(g)) [22]. Except for molecular engineering strategies, combining inorganic fillers with SPEs can also effectively decrease T_g and suppress crystallization [55,70]. On one hand, the fillers can physically disorder the crystallization of polymers. On the other hand, the Lewis acid-base-type interactions between inorganic surface and polymer chains can kinetically inhibit the crystallization and facilitate segmental mobility. Moreover, these Lewis acid–base interactions can further enhance salt dissociation and create more mobile ions.

Despite steadily improved ionic conductivity and intrinsically excellent flexibility [71–73], some important figures of merit limit the efficacy of SPEs in batteries. As the concentration polarization caused by unnecessary anion transport in cells will raise the unwanted charge overpotential and degrade the rate capability, high t^+ is needed to achieve stable Li^+ flux and good electrochemical performance. Unfortunately, unlike SIEs exhibiting t^+ near to be unity [55], most of SPEs have a low t^+ since the dissociated cations and anions are both mobile. For PEO-based SPEs, moreover, the anions tend to move faster than Li^+ because of the strong coordination of Li^+ with the polymer chains, which results in a low t^+ at *ca.* 0.2–0.5. Loosely coordinating SPEs and single-ion-conducting strategy are developed to increase the t^+ [56,74–76], but as a penalty, their capacity to dissociate salts and ionic conductivity are quite reduced. Another challenge of SPEs is their instability to high-voltage cathodes. It is known that the specific energy of a cell is calculated by multiplying the total cathode capacity and the cell voltage and then dividing by the total mass [77]. The narrow electrochemical stability window of PEO-based electrolytes (< 3.8 V) largely restricts their compatibility with high-voltage cathodes, and thus fails to pursue higher energy density. On the contrary, most SIEs exhibit superior performance in the above two aspects, which provides a feasible route to compensate the drawbacks of SPEs by developing IPHEs.

2. 3 Ionic transport in IPHEs

IPHEs have the potential to solve all the issues of SSEs by combining the advantages of both SIEs and SPEs. At the same time, these materials also display more complicated ion transport mechanism than that of any of the single ones. Firstly, the inorganic ceramics can act as a plasticizer to decrease the crystallinity of the polymer matrix, facilitating the mobility of the Li^+-conducting polymer chains [70]. Furthermore, the inorganic component provides abundant Lewis-acid-rich surfaces [26,78]. These acidic sites can immobilize the anions, increasing the t^+ and mitigating the concentration polarization. More importantly, the highly conductive ceramic phase as well as the numerous interphases introduced by inorganic/polymer hybrid architecture creates more effective pathways for fast ion transport [29,79,80].

Given the increased potential ion-conducting routes in IPHEs, great efforts have been made to gain precise insight into their ion transport mechanism, in order to further guide the structural design of IPHEs. Zheng *et al.* [81] developed a symmetric ^{6}Li/IPHE/^{6}Li battery to trace the Li^+ transfer path, in which two ^{6}Li metal electrodes were employed to provide isotopic $^6Li^+$ and replace the $^7Li^+$ in IPHEs during cycling (Fig. 3(a)). By means of solid-state ^{6}Li nuclear magnetic resonance, they provided the first experimental evidence showing that Li^+ preferred the pathway through the LLZO ceramic phase rather than LLZO/PEO interface or PEO matrix in LLZO nanoparticle/PEO IPHE. However, using the same method, Yang *et al.* [82] found that Li^+

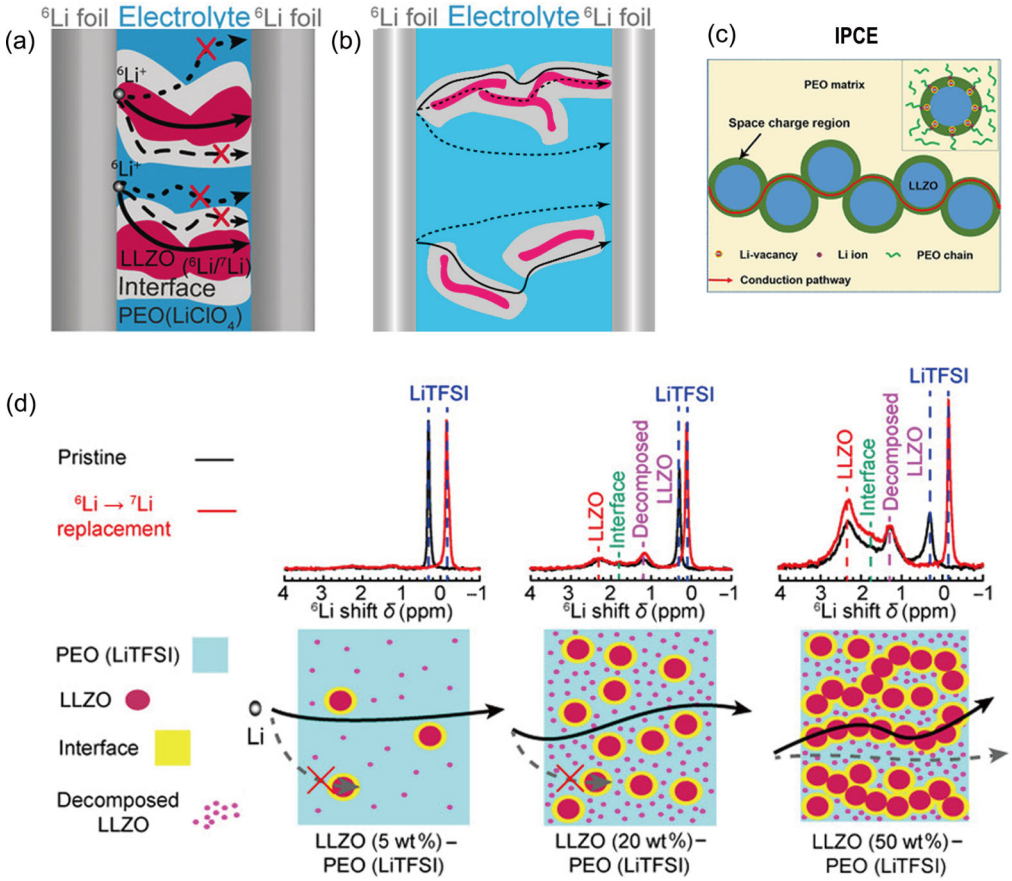

Fig. 3 Illustration of the potential ion transport mechanisms in IPHEs, employing the samples of (a) LLZO particle/PEO system, (b) LLZO nanowire/PAN system, (c) Ga–LLZO nanoparticle/PEO system, and (d) LLZO particle/PEO system with various ceramic filler loading. Reproduced with permission from Ref. [81] for (a), © Wiley-VCH Verlag GmbH & Co. KGaA, Weinheim 2016; Ref. [82] for (b), © American Chemical Society 2017; Ref. [83] for (c), © American Chemical Society 2018; Ref. [86] for (d), © American Chemical Society 2018.

preferred to travel through the modified PAN interface rather than ceramic or polymer phase in LLZO nanowire/PAN IPHE (Fig. 3(b)). Subsequently, both experimental and theoretical investigations revealed the significant role of the ceramic/polymer interphase in fast ion conduction. Via transmission electron microscope, space charge regions of *ca.* 3 nm were observed along the ceramic/polymer interface of Ga–LLZO/PEO IPHE [83]. Different from notorious space-charge layers formed at solid electrolyte/electrode interface and resulting in sluggish interfacial ion transport and dendrite nucleation [84], these space charge regions are generated by defect reaction at ceramic/polymer interface, at which the Li^+ at regular Ga–LLZO lattices move to surface sites and leave the negatively charged vacancies behind in the lattice. Phase-field simulation demonstrated that the fast ion conduction is through these space charge regions and can be facilitated by their percolation (Fig. 3(c)). In parallel, Wang *et al.* [85] found that the LATP fillers in LATP/PEO IPHEs can establish low-energy-barrier Li^+ hopping channels on their surface, where the ionic conductivity was achieved more than twice (measured value) and nearly an order of magnitude (estimated value) higher than that of the LATP pellets (2.0×10^{-4} S·cm^{-1}).

Later, Zheng *et al.* [86] updated their understanding of ion transport path in IPHEs, which demonstrated a strong relation with the concentration of ceramic fillers. As illustrated in Fig. 3(d), Li^+ favors to migrate through the polymer matrix or LLZO/PEO interface at a low LLZO filler content of 5 wt%. With the increase of LLZO amount (up to 50 wt%), the dominant pathway of ion transport shifts from the polymer phase to the ceramic phase, which originates from the formation of continuous ceramic conductive channels with increasing ceramic loadings. Beyond these, Zagórski *et al.* [87] recently pointed out that the polymer phase contributes mainly to the long-range Li^+ transport compared to the

ceramic fillers. With ceramic content of more than 40 vol%, the polymer chains were constrained by ceramic particles, resulting in restricted chain mobility and thus a decreased ionic conductivity.

As above reviewed, the Li^+-conducting pathways in IPHEs involve polymer bulk phase, ceramic bulk phase, and ceramic/polymer interphase. Although the mechanism might be intricate and still controversial, it is undoubted that the composition, concentration, and microstructure synergistically determine the ion-conducting pathway in IPHEs, and the interphase of polymer chains and ceramic fillers plays a key role in creating the fast ion transport channel. Homogeneous dispersion of ceramic fillers and designing judicious architectures to construct sufficient interphases and continuous ion-conducting channels are both effective approaches to improving the ionic conductivity and electrochemical performance of IPHEs for all-solid-state Li batteries. In addition, Li^+ migration across the inorganic/polymer interface (distinct with abovementioned ion transport along interface) can build ion-transport bridge between inorganic and polymer phases and further increase the bulk ionic conductivity of IHPEs. It is also believed that ion exchange between polymer and ceramic phases in IHPEs is conductive to minimize the Li^+ concentration gradient, which can facilitate even Li deposition and mitigate dendrite growth [87]. Regrettably, the ceramic/polymer interface is detected huge resistance, which is ascribed to the high activation energy of Li^+ migration across the interface [88,89]. Although ceramic surface modification has been confirmed to be capable to reduce this barrier [90], research on such direction is still quite lacking. More efforts should be made, including both computational simulation and molecular engineering, to deepen the fundamental understanding of ion exchange at inorganic/polymer interface and facilitate the ion conduction across such heterogeneous interface.

3 Multi-layer architectures for elegant interfacial performance

Interfacial issues are one formidable challenge for all-solid-state Li batteries, including the poor contact, side reactions, Li dendrite growth mainly at the anode/SSE interface, problems of large interfacial impedance caused by the volume change of electrodes, and uncontrolled side reactions caused by the high-voltage decomposition, especially at the cathode/SSE interface [91]. In order to address these issues, IPHEs with multi-layer architectures have become a research hotspot in the recent five years, which can be divided into symmetric sandwich architectures, asymmetric Janus architectures, and cathode/electrolyte integrated architectures.

3.1 Symmetric sandwich architectures

For IPHEs with symmetric sandwich architectures, SPE layers are usually coated on two sides of the hard SIE layer, acting as an artificial soft interphase to improve the interfacial compatibility between electrolyte and two electrodes. A polymer/ceramic/polymer IPHE was proposed by Zhou *et al.* [23], and the schematic is shown in Fig. 4(a). In such architecture, the anion-fixed LATP ceramic layer remarkably blocks the transfer of redox-inactive anions, weakening the concentration polarization across the cell and increasing the rate capability of the battery. Meanwhile, the flexible crosslinked poly(ethylene glycol) methyl ether acrylate (CPMEA) layers provide great wetting with electrodes, leading to more homogeneous Li^+ flux and even Li electrodeposition. As a result, the all-solid-state $LiFePO_4$/Li cell delivered superior long-term electrochemical stability with high Coulombic efficiency of 99.8%–100%. Similarly, Chi *et al*. [92] designed an IPHE with PEO/LLZTO/PEO configuration (Fig. 4(b)), where the LLZTO denoted as Ta-doped LLZO. With the ingenious arrangement and a modified 3D Li anode, the Li/Li symmetrical cell and $LiFePO_4$/Li cell presented a stable voltage profile over 700 h and superior cyclability over 200 h at 90 ℃, respectively. On the contrary, Fig. 4(c) illustrates an opposite symmetric IPHE with inorganic/polymer/inorganic architecture [93]. In this case, two-dimensional (2D) boron nitride nanosheets (BNNSs) were coated on the surface of the PEO middle layer and served as a dense protective layer, granting the PEO electrolyte enhanced mechanical stability and more homogeneous Li^+ flux distribution. The assembled $LiFePO_4$/Li cell showed a specific discharge capacity of 110 $mA \cdot h \cdot g^{-1}$ at 2 C over 200 cycles.

In order to further optimize IPHEs and amplify the merits of the multi-layer architectures, Huo *et al.* [94] designed IPHEs with CIP and PIC composite structures (Fig. 4(d)). Typical CIP structure where a small amount of ceramic particles are dispersed in polymer matrix is claimed to possess good ionic conductivity and interfacial wetting but poor dendrite suppression (Fig. 4(d) middle). When increasing the concentration of ceramic particles, hard ceramic phase becomes the majority and polymer

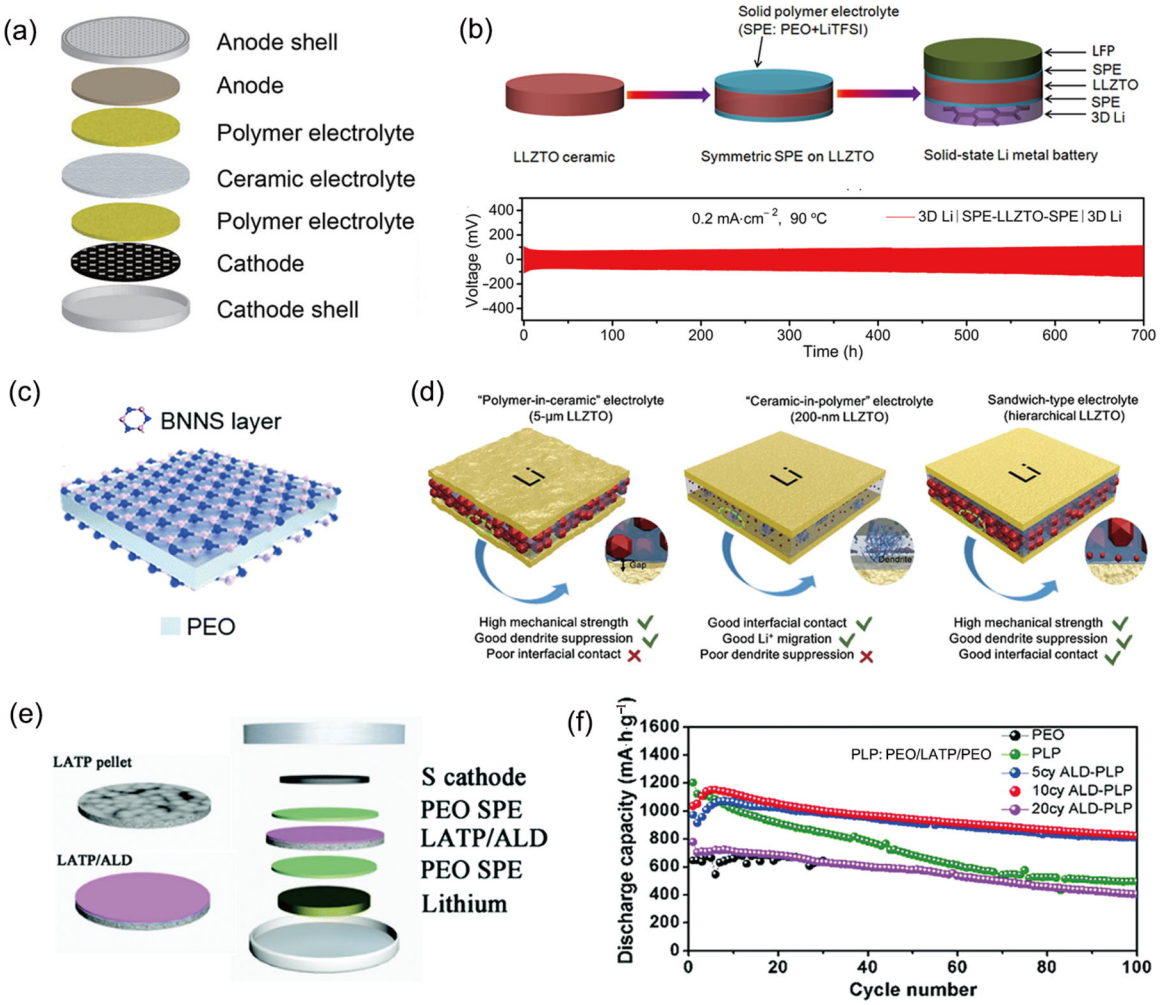

Fig. 4 Multi-layer IPHEs with symmetric sandwish architectures and the corresponding electrochemical performance: (a) illustration of the all-solid-state $LiFePO_4$/Li cell configuration with PEO/LATP/PEO symmetrically layered IPHE; (b) schematic diagram and Li electrodepositon stability of PEO/Ta–LLZO/PEO multi-layer IPHE; (c) illustration of IPHE with a ceramic/polymer/ceramic architecture, where the ceramic layers are systhesized by BN nanosheets ; (d) schematic and property comparison of "polymer-in-ceramic" (PIC, left), "ceramic-in-polymer" (CIP, middle), and hierarchical sandwich-like IPHEs (right); (e, f) schematic illustration of Al_2O_3 atomic layer deposition (ALD)-coated LATP interlayer and all-solid-state Li/S battery with the PEO/ALD-coated LATP/PEO layered IPHE, and its electrochemical performance. Reproduced with permission from Ref. [23] for (a), © American Chemical Society 2016; Ref. [92] for (b), © Elsevier B.V. 2018; Ref. [93] for (c), © The Royal Society of Chemistry 2019; Ref. [94] for (d), © WILEY-VCH Verlag GmbH & Co. KGaA, Weinheim 2019; Ref. [95] for (e, f), © The Royal Society of Chemistry 2018.

electrolyte fills in the gaps of them, constructing the PIC characteristics that exhibit improved mechanical strength and dendrite suppression but poor interfacial contact (Fig. 4(d) left). On this basis, a layered IPHE with a PIC (80 vol% 5 μm LLZTO and 20 vol% PEO) interlayer sandwiched by two CIP (20 vol% 200 nm LLTZO and 80 vol% PEO) layers was constructed (Fig. 4(d) right), simultaneously achieving superior ionic conductivity and interfacial contact (CIP) and enhanced dendrite suppression (PIC). The resulting Li/Li symmetric cells maintained stable plating/stripping cycling after 400 h at 30 ℃, and the $LiFePO_4$/Li cells exhibited good capacity retention of 82.4% after 200 cycles. Using the ALD technique, they further developed a PEO/ALD coated LATP/PEO IPHE and applied it in a Li/S battery that possessed higher energy density (Fig. 4(e)) [95]. The obtained IPHE endowed the Li/S cell with a discharge capacity of 823 $mA{\cdot}h{\cdot}g^{-1}$ after 100 cycles (Fig. 4(f)), which was nearly two times higher than that of the IPHE without an ALD coating or liquid electrolyte. This improvement arises from the soft electrolyte/electrode contact (two polymer layers) and the blocking of the

polysulfide shuttling effect (ceramic interlayer). Moreover, the Al_2O_3 ALD coating also effectively inhibited the reduction of Ti in LATP by the polysulfides.

Gel polymer electrolyte (GPE) consisting of SPE absorbing liquid electrolyte is commonly regarded as a quasi-solid-state electrolyte [96,97]. Although liquid electrolyte additives increase the safety hazard, some studies still introduced GPEs in IPHEs with symmetric sandwich architectures to achieve significantly improved ionic conductivity. For instance, Liu *et al.* [98] fabricated an IPHE of GPE/SIE/GPE to tackle the poor interfacial contact between the garnet Ca/Nb co-doped LLZO (LLCZNO) SIE and electrodes. Due to the extraordinary interfacial contact and high ionic conductivity of the GPE layer, these IPHEs can function at lower temperatures and be more scalable for practical applications.

Symmetric sandwich architectures utilize soft polymer electrolytes to buffer the rigid solid–solid interfaces, avoiding the large interfacial impedance and side reactions between SIEs and electrodes. Meanwhile, the single-ion-conducting nature of SIE effectively blocks anions and enables high t^+, making great contribution to the uniform and fast Li^+ flux across the cells. On this basis, the thickness of polymer layers should be decreased as far as possible, because in SPE layers, the transfer of anions is not blocked as that in SIE layers. In spite of no systematic research, some studies have revealed that layered IPHEs with ultrathin SPE coatings (within 10 μm) exhibited t^+ as high as 0.99 and excellent battery performance [92,99]. Besides, as summarized in Table 1, layered IPHEs composed of pure polymer and ceramic layers exhibit desirable ionic conductivity (10^{-4} S·cm^{-1}) only at high temperatures (≥ 60 ℃) [23,24,92,95], which cannot achieve their good electrochemical performance at RT. The probable reason for the low RT ionic conductivity is the difficulty of ion transport across the polymer/ceramic layer interface and the resulting interfacial impedance [87–89]. Theoretical and experimental studies on breaking through this barrier will be quite beneficial.

Table 1 Electrochemical performance of the representative IPHEs with multi-layer architectures

Layer-by-layer architecture from anode to cathode side	Thickness (μm)	Ionic conductivity (S·cm^{-1})	t^+	Electrochemical window (vs. Li/Li$^+$) (V)	Electrochemical performance in Li metal battery	Ref.
CPMEA/LATP/CPMEA	100/300–500/100	1.0×10^{-4} at 65 ℃	0.89	4.8	102 mA·h·g^{-1} after 640 cycles under 0.6 C at 65 ℃ ($LiFePO_4$ cathode)	[23]
PEO/LLZTO/PEO	8/400/8	1.6×10^{-4} at 60 ℃	—	4.6	135 mA·h·g^{-1} after 200 cycles under 0.2 C at 90 ℃ ($LiFePO_4$ cathode)	[92]
CIP/PIC/CIP	10/40/10	1.6×10^{-4} at 30 ℃	0.47	5.0	100 mA·h·g^{-1} after 200 cycles under 0.1 C at 30 ℃ ($LiFePO_4$ cathode)	[94]
PEO/LATP/Al_2O_3/PEO	70/20/500/70	5.0×10^{-6} at 30 ℃	—	—	823 mA·h·g^{-1} after 100 cycles under 0.1 C at 60 ℃ (S cathode)	[95]
PEO/poly(N-methyl-malonic amide) (PMA)	125/125	1.8×10^{-6} at 30 ℃	0.37	4.8	110 mA·h·g^{-1} after 100 cycles under 0.2 C at 65 ℃ ($LiCoO_2$ cathode)	[100]
PEO/LATP/PAN	15/300/25	6.3×10^{-4} at 60 ℃	0.82	4.5	136 mA·h·g^{-1} after 120 cycles under 0.5 C at 60 ℃ (NCM622 cathode)[a]	[24]
ASHE/LAGP/ CSHE	10/300/10	2.8×10^{-3} at 25 ℃	—	4.7	90 mA·h·g^{-1} after 120 cycles under 0.1 C at 25 ℃ ($LiMnO_2$ cathode)	[101]
(PEO+1% sulfide particles)/LAGP	3/—	2.5×10^{-4} at 30 ℃	0.99	6.0	128 mA·h·g^{-1} after 1000 cycles under 1 C at 60 ℃	[99]
Tough PIC/soft CIP	20/20	8.4×10^{-4} at 25 ℃	0.42	5.0	125 mA·h·g^{-1} after 100 cycles under 0.1 C at 25 ℃ (NCM523 cathode)[a]	[102]
PEO/LLZO/(PEO+separator)/PEO/(PEO+$LiFePO_4$ cathode)	7.5 nm/5.7/25/5.4	1.0×10^{-4} at 55 ℃	—	4.8	151 mA·h·g^{-1} after 120 cycles under 0.2 C at 55 ℃ ($LiFePO_4$ cathode)	[103]
(PEO+LLZO particles)/(PEO+LLZO@C foam S cathode)	20–75	1.1×10^{-4} at 40 ℃	—	—	800 mA·h·g^{-1} after 200 cycles under 0.05 C at 37 ℃ (S cathode)	[25]
(PEO+LLTO nanofibers)/(PEO+carbon nanofiber (CNF)/S cathode)	15	2.3×10^{-4} at 25 ℃	—	4.5	415 mA·h·g^{-1} after 50 cycles under 0.05 C at 25 ℃ (S cathode)	[104]
(PEO+LLZO nanowires)/(PEO+$LiFePO_4$ cathode)	67	2.4×10^{-4} at 25 ℃	—	6.0	159 mA·h·g^{-1} after 80 cycles under 0.1 C at 45 ℃ ($LiFePO_4$ cathode)	[105]

[a] NCM622 and NCM523 correspond to $LiNi_{0.6}Co_{0.2}Mn_{0.2}O_2$ and $LiNi_{0.5}Co_{0.2}Mn_{0.3}O_2$, respectively.

3. 2 Asymmetric Janus architectures

In consideration of the different features of anode and cathode, designing multi-layer IPHEs with asymmetric Janus architectures is another important approach to better serving in diverse electrochemical environments of anode/electrolyte and cathode/electrolyte interfaces. Herein, we begin with a double-layer polymer electrolyte with low-voltage-stable PEO contacting the Li metal anode and high-voltage-stable PMA contacting the cathode (Fig. 5(a)) [100]. This work demonstrates a clear concept that utilizing a Janus architecture can achieve the dendrite-free plating at Li anode and the Li^+ conduction without electrolyte oxidation at high-voltage cathode ($LiCoO_2$). However, due to the absence of anion-fixed SIE layer, the double-layer SPE shows a low t^+ of 0.37, which could induce the generation of space-charge layer and dendrite nucleation. Later, Liang *et al*. [24] developed a Janus multi-layer IPHE by coating PAN and PEO layer onto the cathode and anode sides of LATP electrolyte, respectively (Fig. 5(b)). The incorporation of the LATP ceramic layer tethers the anions and increases the total t^+ up to 0.82. While the upper PAN layer enabled a superior wetting and high-voltage tolerance with cathode, the lower PEO layer protected the LATP from being reduced at anode. Such targeted modification allowed the core LATP layer to better regulate the ion distribution at the interface, restricting the formation of the space-charge layer and Li dendrite nucleation.

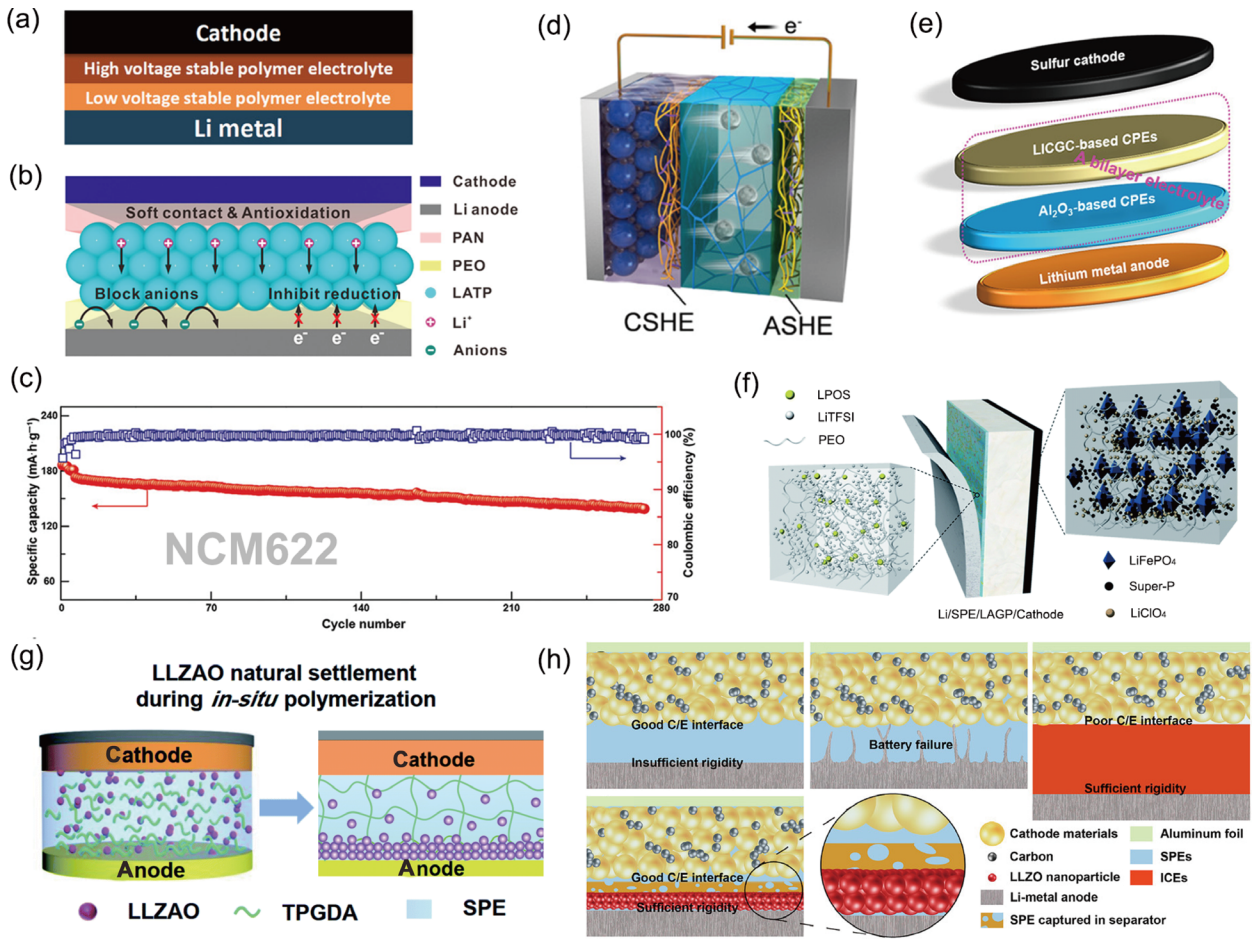

Fig. 5 Multi-layer IPHEs with asymmetric Janus architectures and the corresponding electrochemical performance: (a) illustration of double-layer polymer electrolyte with low-voltage-stable PEO to the anode and high-voltage-stable PMA against the cathode; (b, c) configuration and electrochemical performance of high-voltage Li/NCM622 battery with PEO/LATP/PAN multi-layer IPHE; (d) battery configuration equipped with LAGP electrolyte with Janus self-healing SPE layers. (e) Schematic of Li/S battery with Al_2O_3/PEO and LICGC/PEO Janus double-layer IPHE; (f–h) illustrations showing three other typical asymmetric layered IPHEs. Reproduced with permission from Ref. [100] for (a), © WILEY-VCH Verlag GmbH & Co. KGaA, Weinheim 2018; Ref. [24] for (b), © American Chemical Society 2019; Ref. [106] for (c), © WILEY-VCH Verlag GmbH & Co. KGaA, Weinheim 2019; Ref. [107] for (e), © American Chemical Society 2017; Ref. [99] for (f), © The Royal Society of Chemistry 2017; Ref. [102] for (g), © The Royal Society of Chemistry 2021; Ref. [103] for (h), © American Chemical Society 2017.

They also replaced the LATP interlayer by a flexible 80 wt% LAGP/PAN composite intermediate layer, which could hinder the dendrite penetration and ensure the compact interface [106]. When paired with high-voltage nickel cobalt manganese oxide (NCM622) cathodes, the all-solid-state Li batteries exhibited high capacity and long cycle life (Fig. 5(c)). Recently, self-healing polymer electrolytes (SHEs) were also introduced by Liu *et al.* [101] as Janus interfaces to electrodes due to their ability to spontaneously heal the cracks caused by electrode volume change and maintain the integrated interfacial contacts upon cycling. As shown in Fig. 5(d), SHE layers were constructed on the surfaces of LAGP pellets by *in-situ* polymerizing ureido pyrimidone (UPy)-based monomers in ionic liquid (IL)-based electrolytes on anode side (ASHE) and adiponitrile (AN)-based electrolytes on cathode side (CSHE). While the IL-based ASHE protected the LAGP ceramic from reducing by metallic Li and promotes the formation of stable solid-electrolyte interface (SEI), the AN-based CSHE possessed high resistance against electrochemical oxidation.

Apart from asymmetric IPHEs with two distinct SPEs, there are also some Janus architectures involving only single conductive polymer material. Based on PEO matrix, Judez *et al.* [107] reported a Janus double-layer IPHE with an Al_2O_3/PEO composite layer on Li anode side and a NASICON-type ceramic/PEO composite layer on S cathode in a Li/S battery (Fig. 5(e)). The Al_2O_3 fillers significantly improved the Li anode/electrolyte interfacial properties [108,109], enhancing the cyclability of the Li-based cell; and the layer with NASICON crystal ceramics exhibited high ionic conductivity and high S utilization and cell areal capacity. Meanwhile, the ceramic components in IPHEs could also absorb the polysulfides via chemical bonding and relieve the shuttle effect. Consequently, the Li/S cell possessed a capacity of 518 $mA{\cdot}h{\cdot}g^{-1}$ and 0.53 $mA{\cdot}h{\cdot}cm^{-2}$ with a coulombic efficiency of 99% after 50 cycles. In addition, Zhang *et al.* [99] fabricated a double-layer IPHE by doping $75Li_2S–24P_2S_5–1P_2O_5$ (LPOS) particle mixtures in PEO matrix to form a soft PEO-based electrolyte, and then coating it onto a rigid LAGP pellet layer (Fig. 5(f)). Wang *et al*. [110] also designed a double-layer IPHE consisting of a soft PEO layer and a hard 1%–5% PEO/LAGP layer. The presence of the PEO film on Li anode resulted in satisfactory interface wetting, which decreased the interfacial impedance and prevented Li metal from reacting with LAGP. The $LiFePO_4$/Li cell delivered excellent long-term electrochemical stability with capacity retention of 96.6% after 1000 cycles at 1 C and maintained capacity of 127.8 $mA{\cdot}h{\cdot}g^{-1}$ [99].

Very recently, Zhang *et al*. [102] developed a facile approach to a tough–soft asymmetric thin film, which integrates a ceramic-rich layer on the anode side and a polymer-rich layer on the cathode side. Specifically, a mixed solution of LLZAO powders, polyether monomer, and thermal initiator was directly injected into a 2032 Li battery. Utilizing the natural settlement of LLZAO nanoparticles during *in-situ* polymerization process, the tough–soft as ymmetric IPHE was obtained as schemed in Fig. 5(f). The rigid CIP layer can effectively suppress the growth of Li dendrites, whereas the soft PIC layer can wet the cathode to endow a flexible interface and low interfacial resistance. As a result, the assembled $LiNi_{0.5}Mn_{0.3}Co_{0.2}O_2$/Li batteries exhibit an initial discharge capacity of 149.1 $mA{\cdot}h{\cdot}g^{-1}$ and high cyclic stability at RT.

Last but not least, we introduce a complex multi-layer structural design, which involves not only neat SIE and SPE layers, but also separator and cathode layer with SPE fillers [103]. As shown in Fig. 5(f), on the anode side, a rigid LLZO layer of 5.7 μm was coated with an ultrathin graft PEO-based polymer layer (7.5 nm) to suppress the dendrite growth. On the cathode side, there was an additional two-layer structure including a commercial Celgard 2400 separator and a polymer layer of 5.4 μm. Remarkably, the polymer layer (5.4 μm) spread over the separator and cathode materials, building a continuous electrolyte/cathode interface and an integrated battery structure. Such integrated architecture plays a critical role in lowering the interfacial impedance between cathode and SSEs, and will be further discussed in Section 3.3.

Asymmetric multi-layer IPHEs provide a feasible strategy to satisfy the varied electrochemical environments at cathode and anode interfaces. As aforementioned, some high-voltage-stable polymers have been developed and applied at cathode interface, and blending PEO matrix with high-voltage-resistant oxide SIE fillers (over 5 V) to fabricate composite layers can also widen the electrochemical stability window. Nevertheless, it is still of great significance to exploit qualified SPEs with higher voltage resistance yet without the sacrifice of ionic conductivity, which has potential to thoroughly tackle the interfacial issues of next-generation high-energy-density Li batteries. With regard to mechanical properties, it has been verified that proper toughness

and softness are both indispensable factors for IPHEs to simultaneously achieve Li dendrite inhibition and good contact with electrodes. Therefore, judicious combination and regulation of ceramic-rich PIC layer and polymer-rich CIP layer could be a promising method to be considered. Moreover, it should be noted that the thickness of most multi-layer IPHEs (both symmetric sandwich and asymmetric Janus types) is very thick (100–500 μm, Table 1). However, ideal electrolytes should be as thin as possible to reduce internal resistance and decrease the weight or volume of batteries to achieve higher energy density [111]. Developing approaches to ultrathin SPE layer within 10 μm [71,72] and SIE layer within 50 μm [112–114] are challenging but quite required to obtain thinner IPHE films and put solid-state batteries into commercialization.

3. 3 Electrolyte/cathode integrated architectures

Since both ions and electrons migrate in battery cathodes, improvement of ion-electron-conducting continuum in cathodes is an essential task in pursuit of the long-lasting and high-energy-density Li batteries. In this respect, layered electrolyte/cathode integrated architectures are proposed to accomplish stable and efficient ion-conducting networks inside the cathodes and mitigate the large impedance induced by the numerous interfaces between SSEs and cathode particles.

As shown in Fig. 6(a), Tao *et al.* [25] developed an all-solid-state Li/S battery using an LLZO nanoparticle-

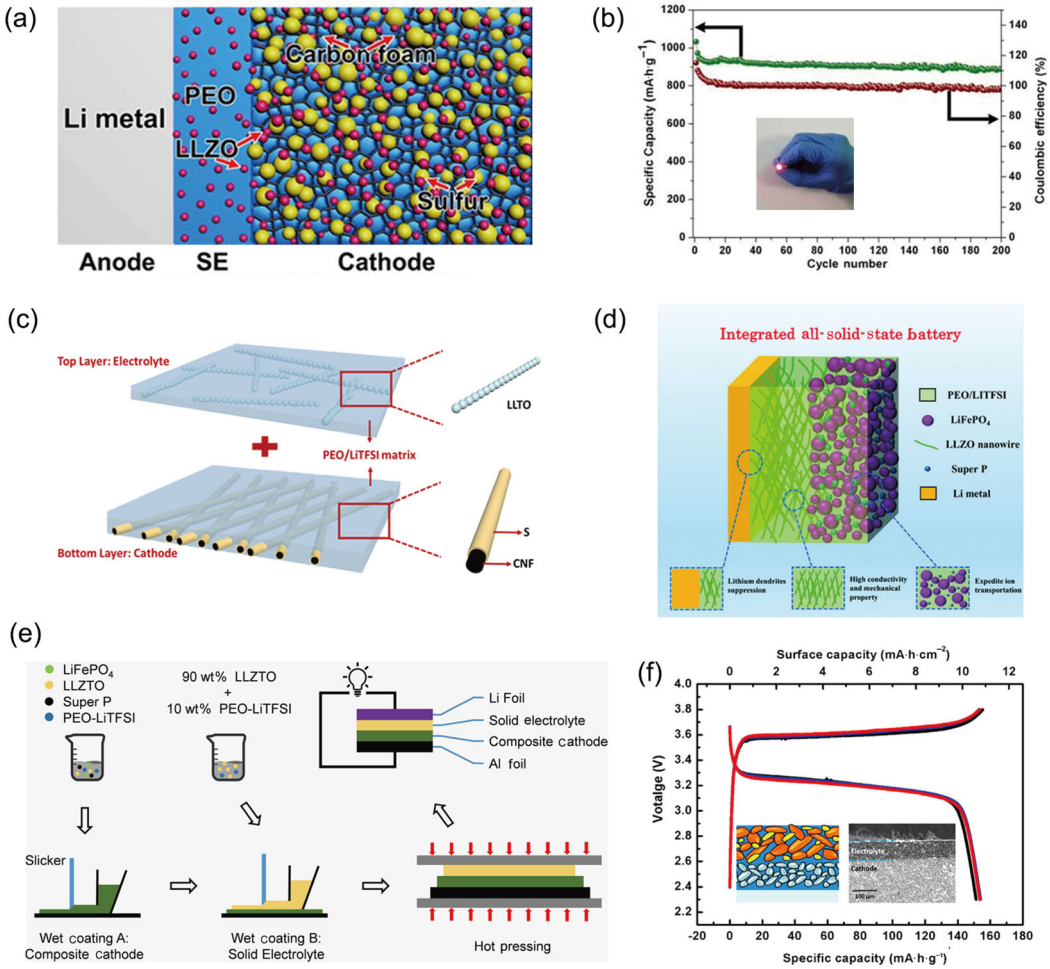

Fig. 6 Multi-layer IPHEs with electrolyte/cathode integrated architectures and the corresponding electrochemical performance: two electrolyte/cathode integrated IPHEs designed for Li/S batteries based on (a, b) LLZO particle/PEO and LLTO nanowire/PEO and (c) electrolytes. The former delivers the specific capacity higher than 900 mA·h·g^{-1} at 37 ℃. (d–f) Schematic diagram, synthetic strategy, and electrochemical performance of three other electrolyte/cathode integrated architectures applied in $LiFePO_4$ batteries. Reproduced with permission from Ref. [25] for (a, b), © American Chemical Society 2017; Ref. [104] for (c), © Elsevier B.V. 2018; Ref. [105] for (d), © WILEY-VCH Verlag GmbH & Co. KGaA, Weinheim 2018; Ref. [115] for (e), © Elsevier B.V. 2018; Ref. [116] for (f), © American Chemical Society 2017.

modified porous carbon (LLZO@C) foam to host the active S host and PEO binders. Then, an LLZO/PEO electrolyte was tightly casted onto the composite S cathode. Such integrated electrolyte and cathode shared the same PEO matrix, significantly reducing the interface resistance between the IPHE and the cathode. Furthermore, the ion-conductive LLZO and PEO existing in cathode increased the ion/electron connectivity and reduced the interfacial resistance between the S material and the ion/electron co-conductive matrix. The assembled cell not only delivered an attractive specific capacity of > 900 $mA \cdot h \cdot g^{-1}$ at human body temperature, but also exhibited high Coulombic efficiency and remarkably stable cycling performance (Fig. 6(b)). Similarly, Zhu *et al.* [104] reported an integrated electrolyte/cathode bi-layer framework with one-dimensional (1D) LLTO nanofiber/PEO electrolyte and 3D CNF/S membranes (Fig. 6(c)). Fast continuous electron/ion transport paths and low interfacial impedance were achieved by permeating the LLTO/PEO IPHE into the pores of the CNF/S cathode.

In addition to Li/S batteries, layered electrolyte/cathode integrated architectures are widely used in other Li batteries. Wan *et al.* [105] fabricated a low-resistance integrated all-solid-state Li battery by using PEO as binders of both $LiFePO_4$ cathode and LLZO nanowire-based IPHE (Fig. 6(d)). On one hand, the uniformly distributed LLZO nanowires increased the ionic conductivity and mechanical strength of the IPHE, leading to even deposition of Li metal and suppression of dendrite growth. On the other hand, the PEO in cathode and IPHE are fused at elevated temperature to form an integrated battery architecture, enhancing the cathode/electrolyte interfacial compatibility and stability. The integrated $LiFePO_4$/IPHE/Li batteries exhibited high specific capacity of 158.7 $mA \cdot h \cdot g^{-1}$ after 80 cycles at 45 ℃. Similar methods adopted by Zha *et al*. [115] and Chen *et al.* [116] PEO-containing $LiFePO_4$ cathodes, SIE filler/PEO IPHEs, and Li anode were stacked layer by layer to form the integrated batteries (Fig. 6(e)). After wet coating and hot pressing, the interfacial resistance of the cathode/electrolyte presented a large decrease from *ca.* 248 to *ca.* 62 $\Omega \cdot cm^{-2}$, which was attributed to the high viscosity and ductility of the compact cathode and electrolyte. One of the assembled full cells achieved an ultrahigh surface discharge capacity of 10.8 $mA \cdot h \cdot cm^{-2}$ and average specific discharge capacity of 155 $mA \cdot h \cdot g^{-1}$ at the current density of 100 $\mu A \cdot cm^{-2}$ at 60 ℃ (Fig. 6(f)) [116].

The above studies proposed a robust battery architecture with outstanding mechanical strength, cathode/electrolyte connectivity, and ion-electron-conducting continuum in cathode. Within such integrated architecture, SPEs serve as not only an ionic conductor but also a structural binder in the IPHE and cathode materials. The increased contact with cathode active materials further emphasizes the significance of enlarging their electrochemical stability window. Simultaneously, SPEs with high t^+, such as anion-tethered single-ion polymer electrolytes, should also be exploited and utilized as the matrix, which could better stabilize the ion flux in IPHE and cathode, and further improve their electrochemical properties.

4 Inorganic/polymer composite structures for efficient ion transport

Compared to stable ion migration at electrolyte/electrode interfaces, efficient and fast ion transport in bulk IPHEs is of equally great significance to improve the electrochemical performance and broaden the working temperature platform for all-solid-state Li batteries. Therefore, numerous inorganic/polymer composite architectures were delicately designed in the past decade. In this section, we systematically review these intellectual achievements according to the shape, distribution, and arrangement of the inorganic components, which is classified into zero-dimensional (0D) particles, 1D or 2D channels, and 3D frameworks.

4.1 0D particles

Doping inorganic particles into the SPE matrix is the most widely studied approach to IPHEs. Generally, the inorganic particles are divided into nonconductive passive fillers (inorganic oxides, metal-organic frameworks, carbonaceous, ferroelectric materials, and others) [117–119] and active SIEs [120–122]. Passive fillers can disorder the crystallization of polymer chains to facilitate the segmental mobility of SPE and create fast ion transport pathway along the filler/polymer interface [70,123–126]. With this regard, increasing filler content to amplify above efficacies should be one effective method to further increase the ionic conductivity. However, due to the nonconductive nature of passive fillers, while increased passive fillers produce larger interfacial area and amorphous SPE phase, the fraction of ion-conductive component decreases at the same time. In contrast, adding active SIE fillers in IPHEs

can increase the interface content and decrease crystallization without sacrificing the conductive phase, which has attracted more attentions than the passive counterpart.

Zhao *et al.* [26] proposed a flexible anion-immobilized IPHE, where the active Al–LLZTO ceramic particles were dispersed in a PEO/Li salt matrix (PLL) (Fig. 7(a)). With the incorporation of LLZTO particles, the anions were effectively immobilized due to their interactions with the ceramic particles. As a result, the PLL electrolyte

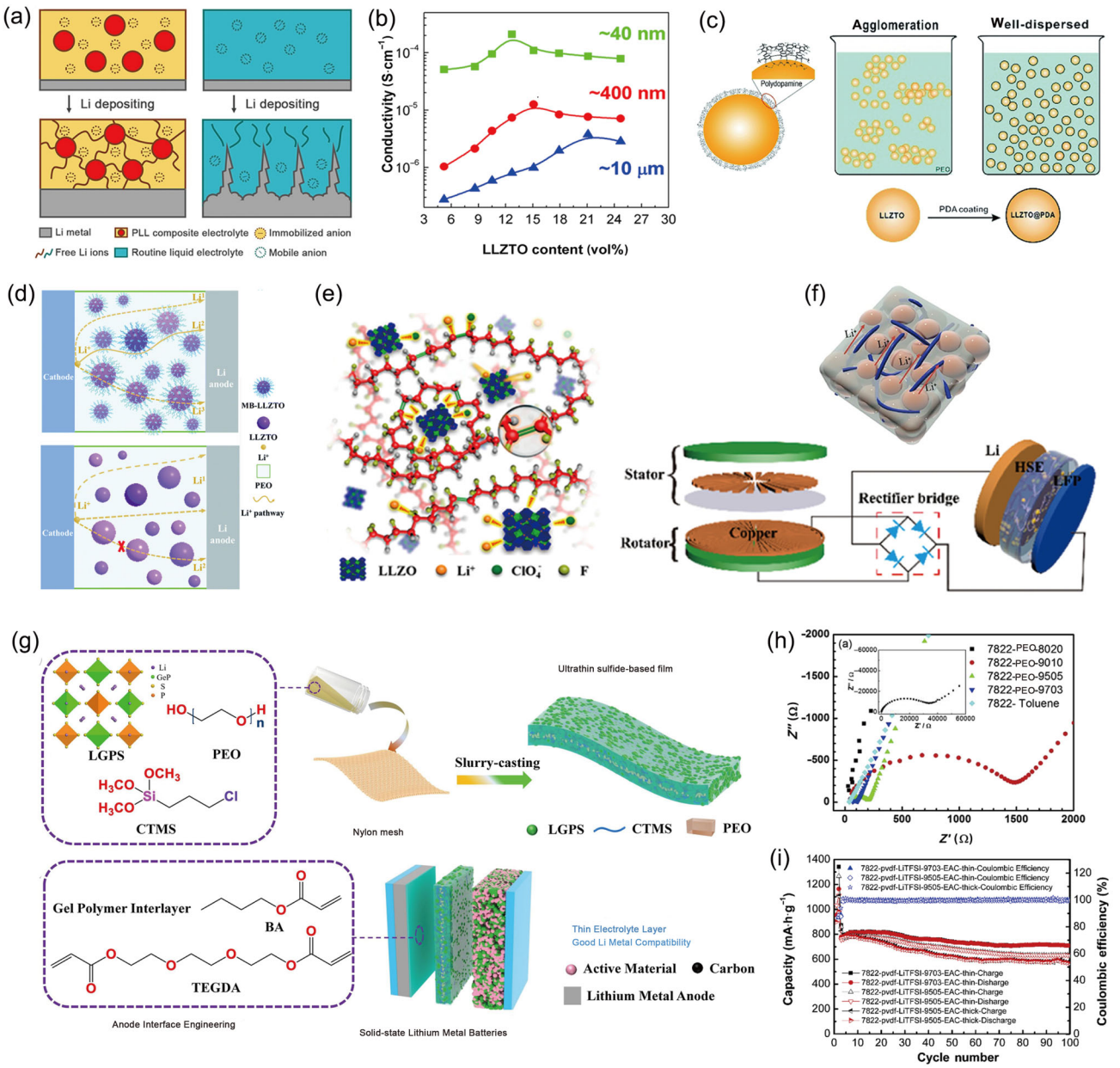

Fig. 7 IPHEs with 0D ceramic particle fillers and the corresponding electrochemical performance: (a) schematic of anion-immobilized IPHE with Al-doped LLZTO fillers and PEO matrix; (b) relationship between ionic conductivity and particle size in IPHE with LLZTO fillers and PEO matrix; schematic diagrams of surface modificaton of oxide ceramic particles by (c) dopamine and (d) molecular brushes (MBs); (e) illustrations and conductivity data of IPHEs based on PVDF-based polymer matrix and (f) their application in mechanical energy harvest; (g) illustration showing a scalable slurry-casting technique towards IPHE with sulfur-based ceramic particles (LGPS) and an interfacial engineering on Li anode; (h) electrochemical impedance spectroscopy and (i) cycling performance of IPHEs with Li_2S–P_2S_5 glass–ceramic SIE fillers. Reproduced with permission from Ref. [79] for (b), © Elsevier Ltd. 2016; Ref. [127] for (c), © The Royal Society of Chemistry 2019; Ref. [128] for (d), © The Royal Society of Chemistry 2019; Ref. [129] for (e), © American Chemical Society 2017; Ref. [130] for (f), 2018 Elsevier Ltd. 2018; Ref. [131] for (g), © Elsevier B.V. 2021; Ref. [122] for (h, i), © Elsevier B.V. 2019.

with 40% LLZTO possessed t^+ as high as 0.58 and desirable ionic conductivity of 1.1×10^{-5} S·cm^{-1} at 25 ℃. The existence of LLZTO particles also improved the mechanical strength to avoid cell short circuiting and broadened the electrochemical window of the PLL to 5.5 V. The $LiFePO_4$/Li cell with the PLL electrolyte rendered a high specific capacity of above 150 mA·h·g^{-1} at 60 ℃. Zhang *et al.* [79] employed Li-salt-free PEO matrix and LLZTO particles to create IPHEs with various particle sizes (Fig. 7(b)). As the Li-salt-free PEO was insulating, ionic conductivity in this system was mainly ascribed to the percolation across the LLZTO/PEO interface. They found that the percolation threshold was strongly coupled to the ceramic particle size. While the IPHE with nano-sized LLZTO (*ca.* 40 nm) showed the highest ionic conductivity of 2.1×10^{-4} S·cm^{-1} at 30 ℃, the IPHEs with micro-sized fillers exhibited ionic conductivity deceasing up to two orders of magnitude.

Good dispersion of nano-sized oxide particles can create much more percolated paths to achieve faster ion conduction. Surface modification engineering could be a useful method to regulate the interfacial behavior of oxide fillers in IPHEs. Huang *et al.* [127] modified the LLZTO surface with dopamine to improve the wettability of LLZTO with PEO, which enabled 80 wt% LLZTO to be uniformly dispersed in 20 wt% PEO matrix without agglomeration (Fig. 7(c)). After modification, the ionic conductivity of IPHEs increased from 6.3×10^{-5} to 1.1×10^{-4} S·cm^{-1} at 30 ℃. Li *et al.* [128] used high-density MBs to modify the LLZTO particles (MB–LLZTO) (Fig. 7(d)). The MBs at the LLZTO surface created fast-conduction domains and the optimal IPHE with 15 wt% MB–LLZTO demonstrated the highest ionic conductivity of 3.1×10^{-4} S·cm^{-1}. Li/S battery was assembled with the IPHE, exhibiting a discharge capacity of *ca.* 1280 mA·h·g^{-1} and stable cycling performance of *ca.* 752 mA·h·g^{-1} after 220 cycles at 45 ℃.

Beyond PEO, other polymer materials can also be applied as the matrix in IPHEs, including PVDF [129], PVC [132], poly(propylene carbonate) (PPC) [133], poly(vinylidene fluoride-co-hexafluoropropylene) (PVDF–HFP) [130], and others [121]. Among them, PVDF is a promising one because of its high ionic conductivity and better electrochemical and mechanical stabilities than those of PEO. By means of first-principles calculation, Zhang *et al.* [129] found that the La atoms of LLZTO could complex with the N atoms and C=O groups of the N,N-dimethylformamide (DMF), behaving as a Lewis base and inducing the chemical dehydrofluorination of the PVDF skeleton. On this basis, they used LLZTO particles to trigger the structural modification of PVDF electrolyte and prepared IPHEs (Fig. 7(e)). As expected, the LLZTO-modified PVDF chains activated the interactions between the polymer matrix, Li salt, and LLZTO fillers, resulting in enhanced mechanical strength, thermostability, and ionic conductivity of *ca.* 5×10^{-4} S·cm^{-1} at 25 ℃. The $LiCoO_2$/Li cell with this IPHE delivered high capacity of 150 mA·h·g^{-1} and good cycling stability (147 mA·h·g^{-1} after 120 cycles) at RT. Similarly, Zhang *et al.* [130] reported an LLZO-incorporated PVDF-HFP IPHE and employed it for mechanical energy harvest (Fig. 7(f)). The assembled $LiFePO_4$/Li cell exhibited discharge capacity of 120 mA·h·g^{-1} at RT (0.5 C) and could efficiently store the pulsed energy.

Due to their higher ionic conductivity and softer mechanical property than oxides, sulfur-based ceramic fillers are also a promising candidate to construct IPHEs. Zheng *et al.* [134] utilized the highly conductive LGPS particles to blend with PEO through ball-milling. They claimed that the oxide conductors, such as LLZO, were too rigid to be closely integrated with PEO, therefore forming limited interface area. In contrast, the soft LGPS can cement better with PEO, and thus produced larger ion-conductive interfaces, exhibiting RT ionic conductivity of 2.2×10^{-4} S·cm^{-1} and good long-term cycling stability against Li metal. With similar ingredients, very recently, Liu *et al.* [131] proposed a scalable slurry-casting technique to explore the mass manufacture of high-performance IPHEs (Fig. 7(g)). Ingenious introduction of a robust nylon mesh as a scaffold enhances the mechanical strength of the IPHE thin films (*ca.* 60 μm) up to 13.8 MPa. Furthermore, interface engineering was employed by *in-situ* polymerization of fluorine-rich gel protective layer on Li anode, which tremendously enhances the compatibility between sulfide IPHE and anode, exhibiting desirable capacity and cyclic performance at RT in high-energy Li/S and Li/NCM622 batteries. In parallel, given the low cost and good electrochemical stability of Li_2S–P_2S_5 glass–ceramic materials, Zhang *et al.* [122] developed a liquid-phase method to synthesize IPHE thin films using $78Li_2S$–$22P_2S_5$ (7822gc) particles, and systematically studied the effects of solvents and SPEs on their microstructure and electrochemical properties. It is found that when the polymer concentration decreases from 20 to 5 wt%, the morphology of SPE

among 7822gc particles changes from micro-fibers to nano- whiskers, resulting in ionic conductivity enhanced by two orders of magnitude (highest at 7.1×10^{-4} $S\cdot cm^{-1}$) (Fig. 7(h)). With such IPHE, the assembled Li/S battery shows a discharge capacity over 700 $mA\cdot h\cdot g^{-1}$ after 100 cycles (90% retention) (Fig. 7(i)) and a 5-fold increase of the cell-based energy density compared to conventional cells with thick SIE pellets.

IPHEs with dispersed 0D SIE particles exhibit improved ionic conductivity, t^+, and electrochemical stability window. More importantly, such physically mixing route is easy to scale up, showing great potential for modern solid-state battery industry. In this case, the mass production of nano-sized yet uniform SIE particles is a crucial prerequisite to implement the ideal performance. In addition, the promoted ionic conductivity, t^+, and electrochemical stability window of such IPHEs rely heavily on the increase of inorganic/polymer interphase or a high ceramic content. Recent research has reported a simultaneous electrospin/electrospray method (electrospin for polymers and electrospray for ceramic particles) that can create IPHE thin films with extremely rich continuous interfaces [135]. Likewise, more effective methods to increase the nanoparticle loading and avoid their agglomeration should be pursued.

4. 2 1D channels and 2D nanosheets

The ongoing research on dispersing ceramic nanoparticles into polymer matrix has been proven to effectively improve ionic conductivity and electrochemical performance. However, these nano-sized fillers with high surface energy are prone to aggregate in polymer matrix, especially at high loads, which decreases the volume fraction of interphase and destroys the percolated interphase network [136]. Besides, the ion transport paths in such IPHEs are always disordered due to the randomly dispersed nanoparticles, decreasing the ion-migration efficiency. In order to tackle these issues, SIE fillers with a continuous surface are established, including nanowires, nanosheets, and aligned structures, which can alleviate the agglomeration and provide more continuous percolated pathway for ion transport.

Liu *et al.* [137] introduced the first case of ceramic nanowire fillers into polymer matrix and compared with the nanoparticle counterpart. As depicted in Figs. 8(a) and 8(b), they found that the 15 wt% LLTO nanowires/PAN IPHEs showed an enhanced ionic conductivity of 2.4×10^{-4} $S\cdot cm^{-1}$ at RT, which was three and two orders of magnitude higher than those of the neat PAN electrolyte (2.1×10^{-7} $S\cdot cm^{-1}$) and 15 wt% LLTO nanoparticles/PAN IPHEs (3.2×10^{-5} $S\cdot cm^{-1}$), respectively. Compared to the isolated LLTO nanoparticles, such progress was attributed to the more efficient ion migration through the conductive network constructed along ceramic nanowire surface, opening a door of novel designs of 1D SIEs. Later, using electrospinning technique, 1D ceramic nanowires including LLTO [138], LLZO [82], and Nb–LLZO [139] were synthesized to create IPHEs in polymer matrix of PEO, PAN, and PMMA, respectively. As expected, all of these materials exhibited elevated RT ionic conductivity on the order of magnitude of 10^{-4} $S\cdot cm^{-1}$.

Furthermore, ceramic nanowires with a well-aligned architecture were proposed by Liu *et al*. [27] and Zhang *et al*. [125]. Compared to randomly-oriented nanowires, as shown in Fig. 8(c), the aligned nanowires along the normal direction of electrodes in polymer matrix displayed one order of magnitude enhancement in ionic conductivity [27], which was caused by the fast ion-conducting pathway without crossing junctions on the surface of the aligned nanowires. Particularly, the surface ionic conductivity along the nanowires was calculated to be a high value of *ca.* 1.3×10^{-2} $S\cdot cm^{-1}$ at 30 ℃, comparable to that of the liquid electrolyte. Alignment provides a novel nano-architectural design for high-efficiency ion conduction, and is further applied in IPHEs with nanoparticle fillers. Zhai *et al.* [140,141] successively vertically aligned LATP and LAGP nanoparticles in PEO matrix via an ice-templating method (Figs. 8(d)–8(f)). At the same time, Liu *et al.* [142] developed a facile approach towards well-aligned ceramic particles through electric field-induced assembly. Under an external alternating-current electric field, LATP nanoparticles and poly(ethylene glycol) diacrylate in poly(dimethylsiloxane) (LATP@PEGDA@PDMS) assembled into necklace-like connected channels (Fig. 8(g)). Owing to the formation of oriented continuous pathway, these IPHEs with aligned ceramic nanoparticles generally exhibited the ionic conductivity 3–7 times higher than that of the random ones.

Ceramic nanosheets can also serve as additives for IPHEs to build the continuous ion-conducting pathway, but the corresponding research is quite limited due to the challenges in large-scale synthesis of qualified nanosheets with fine morphology. By coprecipitation Nb–LLZO with graphene oxide (GO) template, Nb–LLZO nanosheets were prepared for the first time by Song *et al.* [143] (Fig. 8(h)). The IPHE with 15 wt%

Nb–LLZO nanosheets exhibited enhanced ionic conductivity (3.6×10^{-4} S·cm^{-1} at RT) compared to their nanoparticle counterparts (Fig. 8(i)). Moreover, mesoporous lithium aluminate (MLA) nanosheets were also produced by a hydrothermal method, and provided improved ion transport efficiency in IPHEs (Fig. 8(j)) [144].

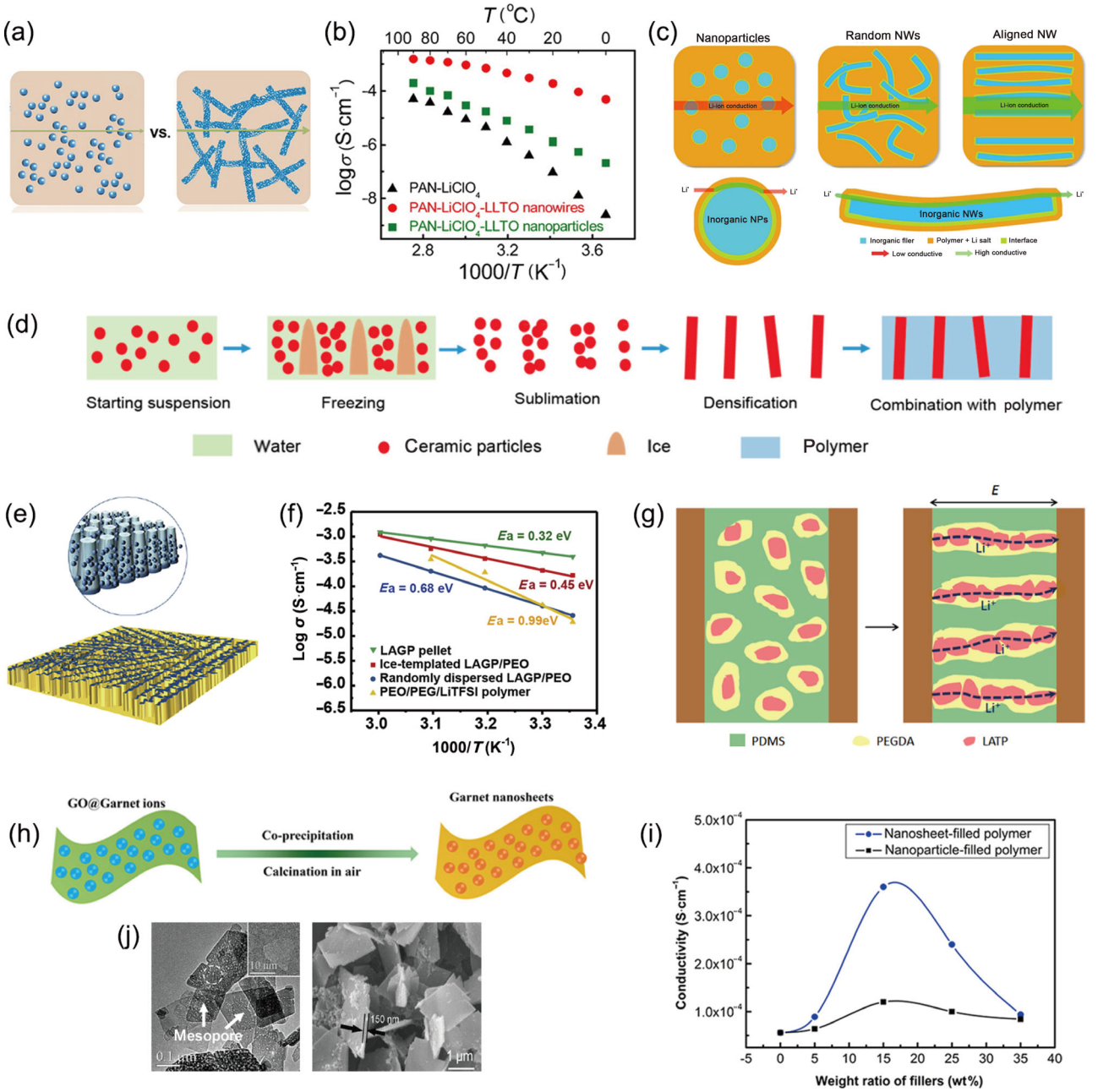

Fig. 8 IPHEs with fillers of 1D ceramic nanowires, aligned channels, and 2D nanosheets, and the corresponding electrochemical performance: (a, b) ionic conductivity comparision and schematic of IPHEs with fillers of LLTO nanowires and nanoparticles; (c) schematic diagrams of ion transport in IPHEs with fillers of nanoparticles, nanowires, and aligned nanowires; illustrations of IPHEs with aligned nanoparticle channels prepared by (d, e) ice-template method, (f) the former's ionic conductivity and (g) electric field-induced assembly; (h) preparation of Nb–LLZO nanosheets and (j) mesoporous $LiAlO_2$ nanosheets, and (i) the former's enhancement in ionic conductivity compared with nanoparticles. Reproduced with permission from Ref. [137] for (a, b), © American Chemical Society 2015; Ref. [27] for (c), © Macmillan Publishers Limited, part of Springer Nature 2017; Ref. [140] for (d), © American Chemical Society 2017; Ref. [141] for (e), © Elsevier Ltd. 2019; Ref. [142] for (g), © American Chemical Society 2018; Ref. [143] for (h), © American Chemical Society 2019; Ref. [144] for (j), © Elsevier B.V. 2007.

Overall, ceramic fillers with shapes of nanowires, nanosheets, and the aligned structures in polymer host can offer continuous ion transport channels, allowing the oriented long-range Li^+ transportation and thus achieving higher ionic conductivity. Synthetic techniques towards high-performance 1D or 2D SIE materials and dispersion methods towards ordered alignment are important areas to be invested.

4. 3 3D continuous frameworks

Evolution from isolated nanoparticle fillers to randomly dispersed nanowires, nanosheets, and further to partially or entirely aligned 1D channels in polymer matrix has been recognized to be able to create continuous ion transport pathway and augment the ion conduction efficiency. On this basis, 3D nanostructured ceramic frameworks filled with SPEs are emerging recently, which can establish 3D long-range ion-conducting channels. In addition to ionic conductivity, the IPHEs with 3D ceramic framework also exhibit enhanced mechanical strength, electrochemical stability window, and long-lasting durability.

A highly sought-after way to such architecture is to evolve the separate nanowires or nanorods to 3D interconnecting ceramic nanofiber framework, and then fill them with polymer electrolytes. Fu *et al*. [28] proposed the first 3D LLZO nanofiber network to provide continuous Li^+ transfer channels in a PEO-based IPHE (Fig. 9(a)). Unlike the conventional blending of ceramic nanowires in polymer matrix, the 3D interconnected network prepared by electrospinning was directly immersed in the Li salt-PEO solution, obtaining a fiber-reinforced polymer composite (FRPC). The FRPC can not only prevent nanofillers' agglomeration but also capture extraordinary mechanical properties. As a result, the flexible FRPC electrolyte membrane exhibited high ionic conductivity of 2.5×10^{-4} S·cm^{-1} at RT, wide electrochemical window up to 6.0 V, and great cycling stability and flame resistance. Later, IPHEs with similar structures were further investigated by varied combinations of 3D ceramic nanofibers and polymers, including LLTO and PEO [145] and LLZO and PVDF systems [146], exhibiting comparable mechanical and electrochemical performance in Li batteries.

Uniquely, Li *et al.* [147] designed an IPHE with LATP/PAN bi-continuous nanofiber 3D network and PEO matrix. The existence of PAN in the nanofiber network can effectively avoid the side reaction between LATP and Li anode since the LATP nanofibers are well-enveloped by the PAN chains. Utilizing analogous PAN-wrapped ceramic nanofibers (Fig. 9(b)), Zhang *et al.* [148] demonstrated that the IPHE consisting of LLZTO/PAN fiber network and PEO matrix exhibited superior battery performance when matching with high-voltage cathodes or operating at RT. Except for improved ionic conductivity through the continuous pathway, the strong oxidation resistance of PAN and LLZTO enlarges the electrochemical stability window from 4.2 V (pure PEO) to 5.2 V. Detectable freely dispersed LLZTO particles further assist to restrict the anion movement and increase the t^+ from 0.24 (PEO matrix) to 0.53. As a result, the assembled $LiNi_{0.5}Mn_{0.3}Co_{0.2}O_2$/Li and $LiCoO_2$/Li batteries delivered reversible capacities of 138.8 and 130.3 mA·h·g^{-1}, respectively, at 0.2 C after 100 cycles. Furthermore, very recently, single-Li^+-conducting polymer electrolyte was employed to replace traditional SPEs to infiltrate into 3D intertwined LATP nanofiber network (Fig. 9(c)) [149]. While composite systems based on PEO fillers exhibit enhanced t^+ of *ca.* 0.4–0.6 only by strong affinity between anions and the acidic groups on surface of ceramics (Table 2), such IPHE shows extraordinary t^+ as high as 0.94 because of the anion insulation of both SPE and SIE components. Meanwhile, continuous ion transport expressway created by LATP nanofibers endows the IPHE with ionic conductivity of 3.1×10^{-4} S·cm^{-1}, overcoming the intrinsic challenge in conductivity of single-ion-conducting SPEs.

As a powerful technique to produce continuous ceramic nanofibers [150–152], electrospinning has been used as a bottom–up method to achieve most of abovementioned 3D nanofiber frameworks. However, taking consideration of the low-cost and large-scale manufacture, such frameworks were also realized by judicious selection of nanofiber templates. Xie *et al.* [153] developed an LLZO nanofiber network derived from bacterial cellulose template, which was a copious natural material and a promising template for engineering porous nanofibers (Fig. 9(d)). The prepared IPHE not only presented enhanced ionic conductivity of 1.1×10^{-4} S·cm^{-1} because of the extended ion transport pathways, but also showed a structural flexibility and enabled minor impedance increase after bending, which could be ascribed to the high length-to-diameter ratio and the intertwined structure of the nanofibers. Furthermore, Gong *et al*. [154,155] developed similar LLZO nanofiber network/PEO hybrid electrolytes using other templates such as cellulose textile and natural wood, exhibiting ionic conductivity of 1×10^{-4}–2×10^{-4} S·cm^{-1} at RT.

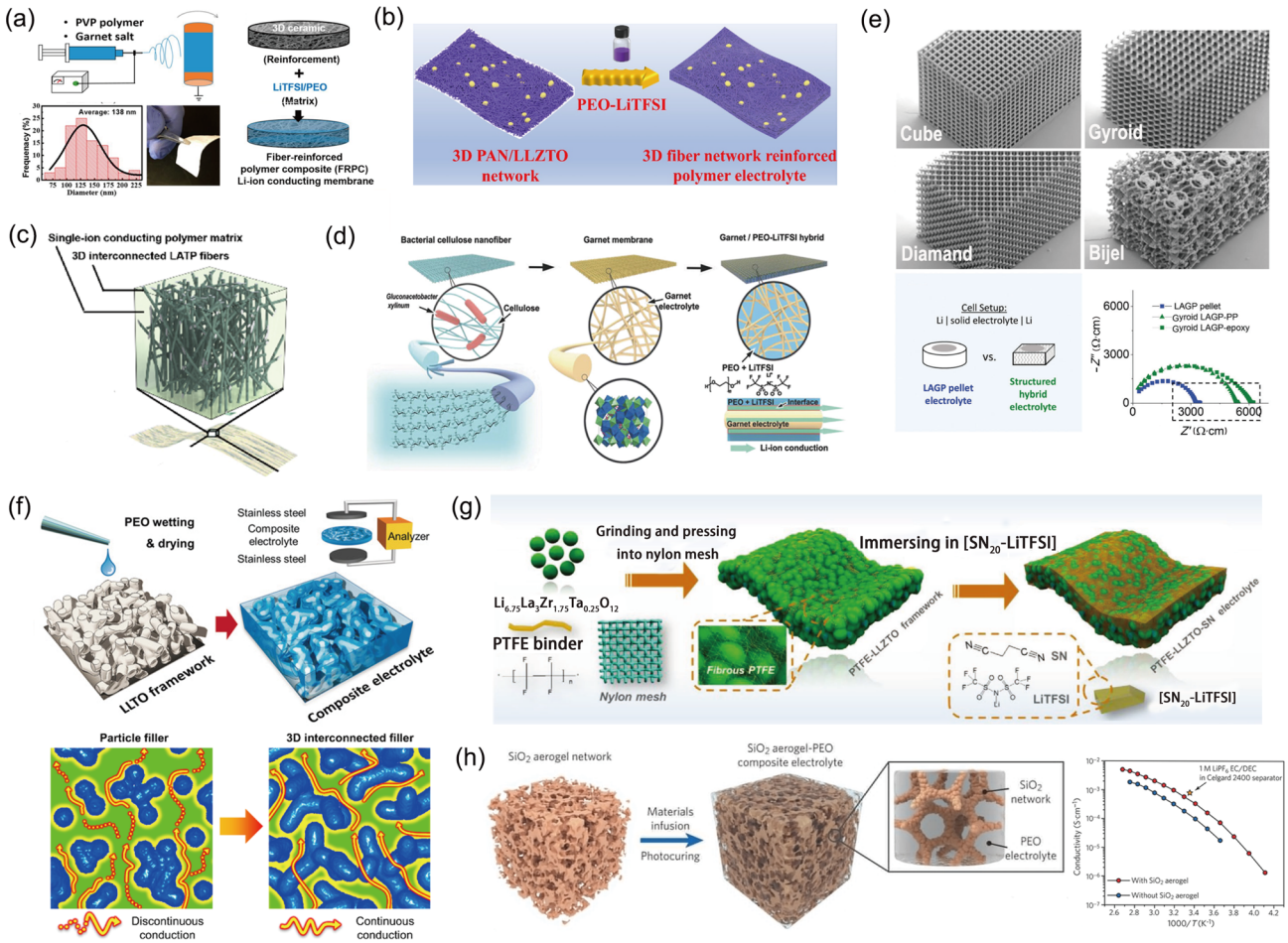

Fig. 9 IPHEs with 3D continuous frameworks and the corresponding electrochemical performance: schematics showing the preparaton of ceramic nanofiber 3D frameworks by eletrospinning and the reinforced IPHEs with (a) LLZO nanofiber/PEO and (b) LLZTO–PAN bi-continuous nanofiber/PEO components; (c) illustration of a single-ion-conducting IPHE consisting single-Li^+-conducting SPE matrix and 3D interconnected LATP fibers; (d) ceramic nanofiber frameworks derived from bacterical cellulose templates as well as the schematic ion transport pathways in these architectures; (e) 3D printing templates with various structures for 3D continuous ceramic frameworks (upper) and the ionic conductivity comparision between IPHE with gyroidal LAGP framework and neat LAGP pellet; (f) schematic of the preparation and ion transport mechanisms of IPHEs with 3D LLTO frameworks derived from hydrogel; (g) simple and solvent-free route towards IPHE with 3D LLZTO-based framework and succinonitrile (SN)-based SPE; (h) illustration of 3D porous SiO_2 aerogel reinforced PEO-based IPHE and its ionic conductivity plot. Reproduced with permission from Ref. [148] for (b), © Elsevier B.V. 2021; Ref. [149] for (c), © The Authors 2021; Ref. [153] for (d), © WILEY-VCH Verlag GmbH & Co. KGaA, Weinheim 2018; Ref. [29] for (e), © The Royal Society of Chemistry 2018; Refs. [136,156] for (f), © WILEY-VCH Verlag GmbH & Co. KGaA, Weinheim 2018, © Elsevier B.V. 2018; Ref. [157] for (g), © WILEY-VCH Verlag GmbH & Co. KGaA, Weinheim 2020; Ref. [78] for (h), © WILEY-VCH Verlag GmbH & Co. KGaA, Weinheim 2018.

Emergence of additive manufacturing (3D printing) affords an efficient approach to ceramic materials with complex morphology [158–160]. Based on this technology, Zekoll *et al.* [29] constructed series of LAGP 3D ordered scaffolds with cubic, gyroidal, diamond, and spinodal (bijel) morphologies (Fig. 9(e)). Filling the empty channels with polypropylene or epoxy created the IPHEs composed of 3D bi-continuous ion-conducting ceramic and insulating polymer microchannels. Owing to the versatile 3D printing platform towards various architectures, the impact of microstructure on the electrical and mechanical properties was readily studied. The gyroidal ceramic framework filled with epoxy exhibited the highest ionic conductivity of 1.6×10^{-4} S·cm^{-1} at RT, which reduced from that of a neat LAGP pellet (2.8×10^{-4} S·cm^{-1}) only by the volume fraction of nonconducting epoxy component. It indicated that the high ionic conductivity of SIEs could

Table 2 Electrochemical performance of the representative IPHEs with various ceramic/polymer composite structures

Composition			Ionic conductivity ($S \cdot cm^{-1}$)	t^+	Electrochemical window (vs. Li/Li^+) (V)	Ref.
Ceramic	SPE	Ceramic content				
0D LLZTO particles	PEO	40 wt%	1.1×10^{-5} at 25 ℃	0.58	5.5	[26]
0D LLZTO particles	Li-salt-free PEO	12 vol%	2.1×10^{-4} at 30 ℃	0.46	4.8	[79]
0D dopamine-modified LLZTO particles	PEO	80 wt%	1.2×10^{-4} at 30 ℃	—	4.8	[127]
0D MB-modified LLZTO particles	PEO	15 wt%	1.6×10^{-4} at 30 ℃	0.39	4.5	[128]
0D LLZTO particles	PVDF	10 wt%	5.0×10^{-4} at 25 ℃	—	—	[129]
0D LLZO particles	PVDF–HFP	50 wt%	1.1×10^{-4} at 25 ℃	0.61	5.3	[130]
0D LGPS particles	PEO	70 wt%	2.2×10^{-4} at 25 ℃	0.41	—	[134]
0D Li_2S–P_2S_5 glass-ceramic particles	PVDF	97 wt%	7.1×10^{-4} at 25 ℃	—	—	[122]
0D LLTO particles	PAN	15 wt%	3.2×10^{-5} at 25 ℃	—	—	[137]
1D LLTO nanowires	PAN	15 wt%	2.4×10^{-4} at 25 ℃	—	5.5	[137]
1D aligned LATP nanoparticles	PEO	40 vol%	5.2×10^{-5} at 25 ℃	—	—	[140]
1D aligned LAGP nanoparticles	PEO	40 vol%	1.7×10^{-4} at 25 ℃	0.56	4.5	[141]
1D aligned LATP/PEO channels	PEGDA/PDMS	—	2.4×10^{-6} at 25 ℃	—	—	[142]
2D Nb–LLZO nanosheets	PEO	15 wt%	3.6×10^{-4} at 25 ℃	—	—	[143]
3D LLZO nanofiber network	PEO	—	$(1.0–3.0)\times10^{-4}$ at 25 ℃	—	6 [28]	[28,121]
3D LATP nanofiber network	Single-Li^+-conducting SPE	—	3.1×10^{-4} at 25 ℃	0.94	5	[149]
3D LATP/PAN bi-continuous nanofiber network	PEO	—	1.0×10^{-4} at 30 ℃	0.32	5	[147]
3D LLZTO/PAN bi-continuous nanofiber network	PEO	12 wt%	1.0×10^{-4} at 30 ℃	0.53	5.2	[148]
3D-printing gyroidal LAGP framework	Li-salt-free epoxy	58 vol%	1.6×10^{-4} at 25 ℃	—	—	[29]
3D LLTO or LLZO framework	PEO	10–44 wt%	$(8.5–8.8)\times10^{-5}$ at 25 ℃	—	4.5 or 5	[136,156]
3D LLZTO framework	PTFE with a nylon mesh	80 wt%	1.2×10^{-4} at 30 ℃	0.53	4.8	[157]
3D SiO_2 aerogel framework	PEO/SN-based SPE	—	6.0×10^{-4} at 30 ℃	0.38	4.4	[78]

be fully exploited by the 3D ceramic framework. Moreover, the gyroid LAGP/epoxy IPHE demonstrated much higher mechanical properties than the fragile LAGP SIE.

Similar 3D ceramic continuous frameworks were forged by Bae *et al.* [136,150] via hydrogel-derived method, and ion-conductive PEO electrolyte was employed to fill the empty channels (Fig. 9(f)). The interconnected 3D LLTO framework provided long-range ion pathways, achieving an ionic conductivity of 8.8×10^{-5} $S \cdot cm^{-1}$ at RT. In addition, the hybridization of rigid ceramic framework and soft polymer matrix endows these materials with great mechanical strength, as well as improved thermal and electrochemical stability. Recently, Jiang *et al.* [157] developed a simple solvent-free method to fabricate a 3D framework composed of LLZTO, polytetrafluoroethylene (PTFE), and light-weight nylon mesh (Fig. 9(g)). Through continuous shear-stress (grinding), PTFE was torn into fibers to adhere the LLZTO powders, leading to a flexible interconnected LLZTO framework. SN-based solid electrolyte was chosen as the organic filler due to its nonflammability, higher ionic conductivity, and better fluidity after melting compared to PEO. The obtained IPHE with ceramic content as high as 80.4 wt% delivers RT ionic conductivity of 1.2×10^{-4} $S \cdot cm^{-1}$, electrochemical stability window of 4.8 V, and t^+ of 0.53, enabling high capacities of 153 and 158 $mA \cdot h \cdot g^{-1}$ and good cyclic stabilities at RT in $LiFePO_4$/Li and $LiNi_{0.5}Mn_{0.3}Co_{0.2}O_2$/Li batteries, respectively.

Except for active 3D ceramic frameworks that can directly conduct Li^+, several IPHEs with passive 3D inorganic frameworks also demonstrate remarkable electrochemical performance. Lin *et al*. [78] introduced a robust mesoporous SiO_2 aerogel as the backbone and filled with a PEO/SN-based polymer matrix (Fig. 8(h)). The interconnected SiO_2 porous aerogel functioned as a robust backbone that strengthened the whole IPHE, which offered large and continuous surfaces with strong anion affinity, creating highly cation-conductive pathways across the composite electrolyte. While the crosslinked-PEO with SN SPE afforded an ionic conductivity of *ca.* 2.0×10^{-4} $S \cdot cm^{-1}$ at 30 ℃, a threefold

enhancement (*ca.* 6.0×10^{-4} S·cm^{-1}) was achieved after combining the SiO_2 aerogel. Consequently, the $LiFePO_4$/Li cell exhibited stable cycling and good rate capability at RT, and even at a lowered temperature (15 ℃), high capacity of *ca.* 105 mA·h·g^{-1} still remained at 0.4 C.

5 Conclusions and perspectives

IPHEs have been regarded as a class of promising electrolyte materials for next-generation high-energy lithium batteries due to their merit integration from today's renowned SIEs and SPEs. Herein, a comprehensive overview of the progress in IPHEs is presented. Although ion-conductive ceramic and polymer components can both provide feasible pathway for the ion conduction, the numerous interphases along ceramic filler surface play a pivotal role in fabricating ion transport pathway with high ionic conductivity and cation transference number. In contrast, ion exchange across the SIE and SPE phases is still limited. Aiming at key issues of SSEs in batteries, advanced IPHE structural design was catalogued and summarized in detail. The multi-layer architectures can be divided into symmetric sandwich, asymmetric Janus, and IPHE/cathode integrated architectures. These layered designs mitigate the interfacial impedance, facilitate the even Li electrodeposition, and improve the high-voltage and long-term stabilities, thus making a great contribution to address the knotty electrode/electrolyte interfacial problems. In parallel, the ceramic/polymer composite structures with inorganic components of 0D nanoparticles, 1D nanowire-aligned channels, 2D nanosheets, and 3D frameworks disorder the crystallization of polymer chains, immobilize the anions, and create fast and continuous ion transport channels, efficiently increasing the ionic conductivity and electrochemical stability windows. Moreover, the combination of hard ceramic and soft polymer materials grants the IPHEs enhancement of both mechanical toughness and flexibility.

Despite booming progress and increasing breakthroughs, the research on IPHEs is still in its infancy. The technical maturity of IPHEs seems to be still insufficient to meet the criteria for the commercialization of all-solid-state Li batteries. Here, we present several major challenges that may appeal to more attention.

1) Comprehensive insight of ion transport mechanisms

IPHEs with two or more components, multi-layer structures, and complicated interfacial areas possess more intricate ion-conducting behavior. Currently, numerous interfaces along ceramic fillers or frameworks have been commonly considered as a fast and efficient pathway for Li^+ migration. However, fundamental understandings of ion transport across inorganic/polymer interfaces, between multiple layers, and between IPHEs and electrodes are quite limited. More advanced characterization and computational simulation technologies should be applied to study these mechanisms, including both thermodynamic and kinetic processes, which can better guide the material design and solve the intrinsic problems of IPHEs to fabricate high-performance all-solid-state Li batteries.

2) Stable electrolyte/electrode interfaces at higher energy and current density

At present, most of the IPHEs operate in low-voltage $LiFPO_4$ cells, while a few can match with high-voltage NCM cathodes. This is mainly owing to the narrow electrochemical stability window of the polymer components. With this regard, developing SPEs with broader electrochemical stability window is of great significance to fulfill the requests of more powerful all-solid-state batteries such as Li/NCM, Li/S, and even Li/air batteries. In addition, increased current density and electrodeposition capacity tend to destroy the interface stability at Li anodes, further highlighting the demands of more stable IPHEs for batteries with higher capacity and rate.

3) Eligible ionic conductivity at RT and lower temperature scope

Electric vehicles, wearable electronics, and intelligent machines put batteries closer into human life, irritating the need for battery materials that can function at RT and even lower temperatures. However, the majority of ongoing research still need to conduct electrochemical tests at high temperatures. This is because the RT ionic conductivity of most IPHEs is still at 10^{-4} S·cm^{-1} order of magnitude, albeit very few ones can reach the value near to 10^{-3} S·cm^{-1}. Fabricating aligned channels or 3D continuous ceramic frameworks to form ion transport expressway is an attractive strategy to improve the ionic conductivity. Machine learning and high throughput could be used to assist the design, discovery, and screening of IPHEs. The emerging 3D printing techniques that can achieve complex structure manufacture could also make great contribution.

4) Ultrathin, flexible yet robust films for light and safe batteries

The thicknesses of many current IPHEs (100–500 μm)

are much larger than the commercial liquid electrolyte/separator system (*ca.* 10 μm), severely limiting their volume energy density. Simultaneously, more and more advanced EES devices have been implanted in not only space vehicles and unmanned drones, but also our clothing, skin, and even bodies, placing desperate demand for light, safe, and energy dense batteries. Thus, ultrathin, flexible, but mechanically robust IPHE films should be further exploited. Moreover, low-cost and large-scale manufacture for commercialization should also be considered. It is known that most of SIEs with high ionic conductivity consume the rare metal resources and exhibit poor mechanical compliance. Judicious design towards IPHEs with less expensive elements, facile synthetic procedures, and good processing compatibility with modern battery industry is indispensable.

Acknowledgements

This work was financially supported by the National Natural Science Foundation of China (No. 22003017), the National Key R&D Program of China (No. 2018YFB1900603), and Natural Science Foundation of Guangdong Province (No. 2020A1515011506). Xiaoyu JI is thankful for the financial support from the China Scholarship Council (No. 201903170199) for his visit to Yale University. The authors thank Prof. Mingjiang ZHONG (Yale University) and Prof. Stephen Z. D. CHENG (University of Akron) for their helpful discussion.

References

[1] Cano ZP, Banham D, Ye S, *et al*. Batteries and fuel cells for emerging electric vehicle markets. *Nat Energy* 2018, **3**: 279–289.

[2] Dunn B, Kamath H, Tarascon J-M. Electrical energy storage for the grid: A battery of choices. *Science* 2011, **334**: 928–935.

[3] Chu B, Burnett W, Chung JW, *et al*. Bring on the bodyNET. *Nature* 2017, **549**: 328–330.

[4] Wang MQ, Vecchio D, Wang CY, *et al*. Biomorphic structural batteries for robotics. *Sci Robot* 2020, **5**: eaba1912.

[5] Manthiram A, Yu X, Wang S. Lithium battery chemistries enabled by solid-state electrolytes. *Nat Rev Mater* 2017, **2**: 16103.

[6] Janek J, Zeier WG. A solid future for battery development. *Nat Energy* 2016, **1**: 16141.

[7] Robinson AL, Janek J. Solid-state batteries enter EV fray. *MRS Bull* 2014, **39**: 1046–1047.

[8] Choi JW, Aurbach D. Promise and reality of post-lithium-ion batteries with high energy densities. *Nat Rev Mater* 2016, **1**: 16013.

[9] Bruce PG, Freunberger SA, Hardwick LJ, *et al*. Li–O_2 and Li–S batteries with high energy storage. *Nat Mater* 2012, **11**: 19–29.

[10] Bruce PG. *Solid State Electrochemistry*. Cambridge, UK: Cambridge University Press, 1995.

[11] Cheng XB, Zhang R, Zhao CZ, *et al*. A review of solid electrolyte interphases on lithium metal anode. *Adv Sci* 2016, **3**: 1500213.

[12] Cao DX, Sun X, Li Q, *et al*. Lithium dendrite in all-solid-state batteries: Growth mechanisms, suppression strategies, and characterizations. *Matter* 2020, **3**: 57–94.

[13] Zhao Q, Stalin S, Zhao C-Z, *et al*. Designing solid-state electrolytes for safe, energy-dense batteries. *Nat Rev Mater* 2020, **5**: 229–252.

[14] Wang XE, Kerr R, Chen FF, *et al*. Toward high-energy-density lithium metal batteries: Opportunities and challenges for solid organic electrolytes. *Adv Mater* 2020, **32**: 1905219.

[15] Gao ZH, Sun HB, Fu L, *et al*. Promises, challenges, and recent progress of inorganic solid-state electrolytes for all-solid-state lithium batteries. *Adv Mater* 2018, **30**: 1705702.

[16] Famprikis T, Canepa P, Dawson JA, *et al*. Fundamentals of inorganic solid-state electrolytes for batteries. *Nat Mater* 2019, **18**: 1278–1291.

[17] Hallinan Jr DT, Balsara NP. Polymer electrolytes. *Annu Rev Mater Res* 2013, **43**: 503–525.

[18] Zhou D, Shanmukaraj D, Tkacheva A, *et al*. Polymer electrolytes for lithium-based batteries: Advances and prospects. *Chem* 2019, **5**: 2326–2352.

[19] Wu JL, Xu F, Li SM, *et al*. Porous polymers as multifunctional material platforms toward task-specific applications. *Adv Mater* 2019, **31**: 1802922.

[20] Stephan AM, Nahm KS. Review on composite polymer electrolytes for lithium batteries. *Polymer* 2006, **47**: 5952–5964.

[21] Liu YJ, Li C, Li BJ, *et al*. Germanium thin film protected lithium aluminum germanium phosphate for solid-state Li batteries. *Adv Energy Mater* 2018, **8**: 1702374.

[22] Lopez J, Mackanic DG, Cui Y, *et al*. Designing polymers for advanced battery chemistries. *Nat Rev Mater* 2019, **4**: 312–330.

[23] Zhou WD, Wang SF, Li YT, *et al*. Plating a dendrite-free lithium anode with a polymer/ceramic/polymer sandwich electrolyte. *J Am Chem Soc* 2016, **138**: 9385–9388.

[24] Liang J-Y, Zeng X-X, Zhang X-D, *et al*. Engineering Janus interfaces of ceramic electrolyte via distinct functional polymers for stable high-voltage Li-metal batteries. *J Am Chem Soc* 2019, **141**: 9165–9169.

[25] Tao XY, Liu YY, Liu W, *et al*. Solid-state lithium–sulfur batteries operated at 37 ℃ with composites of nanostructured $Li_7La_3Zr_2O_{12}$/carbon foam and polymer. *Nano Lett* 2017, **17**: 2967–2972.

[26] Zhao C-Z, Zhang X-Q, Cheng X-B, *et al*. An anion-immobilized composite electrolyte for dendrite-free lithium

metal anodes. *Proc Natl Acad Sci USA* 2017, **114**: 11069–11074.

[27] Liu W, Lee SW, Lin D, *et al*. Enhancing ionic conductivity in composite polymer electrolytes with well-aligned ceramic nanowires. *Nat Energy* 2017, **2**: 17035.

[28] Fu KK, Gong YH, Dai JQ, *et al*. Flexible, solid-state, ion-conducting membrane with 3D garnet nanofiber networks for lithium batteries. *Proc Natl Acad Sci USA* 2016, **113**: 7094–7099.

[29] Zekoll S, Marriner-Edwards C, Hekselman AKO, *et al*. Hybrid electrolytes with 3D bicontinuous ordered ceramic and polymer microchannels for all-solid-state batteries. *Energy Environ Sci* 2018, **11**: 185–201.

[30] Liu XY, Li XR, Li HX, *et al*. Recent progress of hybrid solid-state electrolytes for lithium batteries. *Chem A Eur J* 2018, **24**: 18293–18306.

[31] Zheng Y, Yao YZ, Ou JH, *et al*. A review of composite solid-state electrolytes for lithium batteries: Fundamentals, key materials and advanced structures. *Chem Soc Rev* 2020, **49**: 8790–8839.

[32] Li S, Zhang S-Q, Shen L, *et al*. Progress and perspective of ceramic/polymer composite solid electrolytes for lithium batteries. *Adv Sci* 2020, **7**: 1903088.

[33] Bruce PG, West AR. The A–C conductivity of polycrystalline LISICON, $Li_{2+2x}Zn_{1-x}GeO_4$, and a model for intergranular constriction resistances. *J Electrochem Soc* 1983, **130**: 662–669.

[34] Arbi K, Rojo JM, Sanz J. Lithium mobility in titanium based Nasicon $Li_{1+x}Ti_{2-x}Al_x(PO_4)_3$ and $LiTi_{2-x}Zr_x(PO_4)_3$ materials followed by NMR and impedance spectroscopy. *J Eur Ceram Soc* 2007, **27**: 4215–4218.

[35] Knauth P. Inorganic solid Li ion conductors: An overview. *Solid State Ion* 2009, **180**: 911–916.

[36] Zhao YS, Daemen LL. Superionic conductivity in lithium-rich anti-perovskites. *J Am Chem Soc* 2012, **134**: 15042–15047.

[37] Thangadurai V, Narayanan S, Pinzaru D. Garnet-type solid-state fast Li ion conductors for Li batteries: Critical review. *Chem Soc Rev* 2014, **43**: 4714–4727.

[38] Kamaya N, Homma K, Yamakawa Y, *et al*. A lithium superionic conductor. *Nat Mater* 2011, **10**: 682–686.

[39] Hayashi A, Hama S, Morimoto H, *et al*. Preparation of Li_2S–P_2S_5 amorphous solid electrolytes by mechanical milling. *J Am Ceram Soc* 2001, **84**: 477–479.

[40] Zhang YB, Chen RJ, Liu T, *et al*. High capacity, superior cyclic performances in all-solid-state lithium-ion batteries based on $78Li_2S$–$22P_2S_5$ glass–ceramic electrolytes prepared via simple heat treatment. *ACS Appl Mater Interfaces* 2017, **9**: 28542–28548.

[41] Bachman JC, Muy S, Grimaud A, *et al*. Inorganic solid-state electrolytes for lithium batteries: Mechanisms and properties governing ion conduction. *Chem Rev* 2016, **116**: 140–162.

[42] Zhang BK, Tan R, Yang LY, *et al*. Mechanisms and properties of ion-transport in inorganic solid electrolytes. *Energy Storage Mater* 2018, **10**: 139–159.

[43] Wang Y, Richards WD, Ong SP, *et al*. Design principles for solid-state lithium superionic conductors. *Nat Mater* 2015, **14**: 1026–1031.

[44] Xu HH, Wang SF, Wilson H, *et al*. Y-doped NASICON-type $LiZr_2(PO_4)_3$ solid electrolytes for lithium-metal batteries. *Chem Mater* 2017, **29**: 7206–7212.

[45] He X, Zhu Y, Mo Y. Origin of fast ion diffusion in super-ionic conductors. *Nat Commun* 2017, **8**: 15893.

[46] Zhao N, Khokhar W, Bi ZJ, *et al*. Solid garnet batteries. *Joule* 2019, **3**: 1190–1199.

[47] Kato Y, Hori S, Saito T, *et al*. High-power all-solid-state batteries using sulfide superionic conductors. *Nat Energy* 2016, **1**: 16030.

[48] Bocharova V, Sokolov AP. Perspectives for polymer electrolytes: A view from fundamentals of ionic conductivity. *Macromolecules* 2020, **53**: 4141–4157.

[49] Sun J, Stone GM, Balsara NP, *et al*. Structure–conductivity relationship for peptoid-based PEO–mimetic polymer electrolytes. *Macromolecules* 2012, **45**: 5151–5156.

[50] Wu JH, Liu SF, Han FD, *et al*. Lithium/sulfide all-solid-state batteries using sulfide electrolytes. *Adv Mater* 2021, **33**: 2000751.

[51] Li X, Ren ZH, Norouzi Banis M, *et al*. Unravelling the chemistry and microstructure evolution of a cathodic interface in sulfide-based all-solid-state Li-ion batteries. *ACS Energy Lett* 2019, **4**: 2480–2488.

[52] Wu JH, Shen L, Zhang ZH, *et al*. All-solid-state lithium batteries with sulfide electrolytes and oxide cathodes. *Electrochem Energy Rev* 2021, **4**: 101–135.

[53] Wright PV. Electrical conductivity in ionic complexes of poly(ethylene oxide). *Brit Polym J* 1975, **7**: 319–327.

[54] Xue ZG, He D, Xie XL. Poly(ethylene oxide)-based electrolytes for lithium-ion batteries. *J Mater Chem A* 2015, **3**: 19218–19253.

[55] Fan L-Z, He HC, Nan C-W. Tailoring inorganic–polymer composites for the mass production of solid-state batteries. *Nat Rev Mater* 2021, **6**: 1003–1019.

[56] Mindemark J, Lacey MJ, Bowden T, *et al*. Beyond PEO—Alternative host materials for Li^+-conducting solid polymer electrolytes. *Prog Polym Sci* 2018, **81**: 114–143.

[57] Gadjourova Z, Andreev YG, Tunstall DP, *et al*. Ionic conductivity in crystalline polymer electrolytes. *Nature* 2001, **412**: 520–523.

[58] Stoeva Z, Martin-Litas I, Staunton E, *et al*. Ionic conductivity in the crystalline polymer electrolytes PEO_6:$LiXF_6$, X = P, As, Sb. *J Am Chem Soc* 2003, **125**: 4619–4626.

[59] Cheng S, Li XW, Zheng YW, *et al*. Anisotropic ion transport in 2D polymer single crystal-based solid polymer electrolytes. *Giant* 2020, **2**: 100021.

[60] Bannister DJ, Davies GR, Ward IM, *et al*. Ionic conductivities of poly(methoxy polyethylene glycol monomethacrylate) complexes with $LiSO_3CH_3$. *Polymer* 1984, **25**: 1600–1602.

[61] Ji XY, Cao MX, Fu XW, *et al*. Efficient room-temperature solid-state lithium ion conductors enabled by mixed-graft block copolymer architectures. *Giant* 2020, **3**: 100027.

[62] Khurana R, Schaefer JL, Archer LA, *et al*. Suppression of lithium dendrite growth using cross-linked polyethylene/poly(ethylene oxide) electrolytes: A new approach for practical lithium-metal polymer batteries. *J Am Chem Soc* 2014, **136**: 7395–7402.

[63] Zheng YW, Li XW, Li CY. A novel de-coupling solid polymer electrolyte via semi-interpenetrating network for lithium metal battery. *Energy Storage Mater* 2020, **29**: 42–51.

[64] Wang HC, Wang Q, Cao X, *et al*. Thiol-branched solid polymer electrolyte featuring high strength, toughness, and lithium ionic conductivity for lithium-metal batteries. *Adv Mater* 2020, **32**: 2001259.

[65] Hawker CJ, Chu FK, Pomery PJ, *et al*. Hyperbranched poly(ethylene glycol)s: A new class of ion-conducting materials. *Macromolecules* 1996, **29**: 3831–3838.

[66] Shibuya Y, Tatara R, Jiang Y, *et al*. Brush-first ROMP of poly(ethylene oxide) macromonomers of varied length: Impact of polymer architecture on thermal behavior and Li^+ conductivity. *J Polym Sci A Polym Chem* 2019, **57**: 448–455.

[67] Bennington P, Deng CT, Sharon D, *et al*. Role of solvation site segmental dynamics on ion transport in ethylene-oxide based side-chain polymer electrolytes. *J Mater Chem A* 2021, **9**: 9937–9951.

[68] Deng CT, Webb MA, Bennington P, *et al*. Role of molecular architecture on ion transport in ethylene oxide-based polymer electrolytes. *Macromolecules* 2021, **54**: 2266–2276.

[69] Ji XY, Li SM, Cao MX, *et al*. Crosslinked polymer-brush electrolytes: An approach to safe all-solid-state lithium metal batteries at room temperature. *Batter Supercaps* 2022, **5**: e202100319.

[70] Croce F, Appetecchi GB, Persi L, *et al*. Nanocomposite polymer electrolytes for lithium batteries. *Nature* 1998, **394**: 456–458.

[71] Zhou MH, Liu RL, Jia DY, *et al*. Ultrathin yet robust single lithium-ion conducting quasi-solid-state polymer-brush electrolytes enable ultralong-life and dendrite-free lithium-metal batteries. *Adv Mater* 2021, **33**: 2100943.

[72] Wang ZY, Shen L, Deng SG, *et al*. 10 μm-thick high-strength solid polymer electrolytes with excellent interface compatibility for flexible all-solid-state lithium-metal batteries. *Adv Mater* 2021, **33**: 2100353.

[73] Mackanic DG, Yan X, Zhang Q, *et al*. Decoupling of mechanical properties and ionic conductivity in supramolecular lithium ion conductors. *Nat Commun* 2019, **10**: 5384.

[74] Cowie JMG, Spence GH. Novel single ion, comb-branched polymer electrolytes. *Solid State Ion* 1999, **123**: 233–242.

[75] Porcarelli L, Shaplov AS, Salsamendi M, *et al*. Single-ion block copoly(ionic liquid)s as electrolytes for all-solid state lithium batteries. *ACS Appl Mater Interfaces* 2016, **8**: 10350–10359.

[76] Ma Q, Zhang H, Zhou CW, *et al*. Single lithium-ion conducting polymer electrolytes based on a super-delocalized polyanion. *Angew Chem Int Ed* 2016, **55**: 2521–2525.

[77] Liu J, Bao Z, Cui Y, *et al*. Pathways for practical high-energy long-cycling lithium metal batteries. *Nat Energy* 2019, **4**: 180–186.

[78] Lin DC, Yuen PY, Liu YY, *et al*. A silica-aerogel-reinforced composite polymer electrolyte with high ionic conductivity and high modulus. *Adv Mater* 2018, **30**: 1802661.

[79] Zhang JX, Zhao N, Zhang M, *et al*. Flexible and ion-conducting membrane electrolytes for solid-state lithium batteries: Dispersion of garnet nanoparticles in insulating polyethylene oxide. *Nano Energy* 2016, **28**: 447–454.

[80] Wu N, Chien P-H, Qian YM, *et al*. Enhanced surface interactions enable fast Li^+ conduction in oxide/polymer composite electrolyte. *Angew Chem Int Ed* 2020, **59**: 4131–4137.

[81] Zheng J, Tang MX, Hu Y-Y. Lithium ion pathway within $Li_7La_3Zr_2O_{12}$–polyethylene oxide composite electrolytes. *Angew Chem Int Ed* 2016, **55**: 12538–12542.

[82] Yang T, Zheng J, Cheng Q, *et al*. Composite polymer electrolytes with $Li_7La_3Zr_2O_{12}$ garnet-type nanowires as ceramic fillers: Mechanism of conductivity enhancement and role of doping and morphology. *ACS Appl Mater Interfaces* 2017, **9**: 21773–21780.

[83] Li Z, Huang H-M, Zhu J-K, *et al*. Ionic conduction in composite polymer electrolytes: Case of PEO:Ga–LLZO composites. *ACS Appl Mater Interfaces* 2019, **11**: 784–791.

[84] Wang L, Xie R, Chen B, *et al*. *In-situ* visualization of the space-charge-layer effect on interfacial lithium-ion transport in all-solid-state batteries. *Nat Commun* 2020, **11**: 5889.

[85] Wang WM, Yi E, Fici AJ, *et al*. Lithium ion conducting poly(ethylene oxide)-based solid electrolytes containing active or passive ceramic nanoparticles. *J Phys Chem C* 2017, **121**: 2563–2573.

[86] Zheng J, Hu Y-Y. New insights into the compositional dependence of Li-ion transport in polymer–ceramic composite electrolytes. *ACS Appl Mater Interfaces* 2018, **10**: 4113–4120.

[87] Zagórski J, López del Amo JM, Cordill MJ, *et al*. Garnet–polymer composite electrolytes: New insights on local Li-ion dynamics and electrodeposition stability with Li metal anodes. *ACS Appl Energy Mater* 2019, **2**: 1734–1746.

[88] Langer F, Palagonia MS, Bardenhagen I, *et al*. Impedance spectroscopy analysis of the lithium ion transport through the $Li_7La_3Zr_2O_{12}$/$P(EO)_{20}Li$ interface. *J Electrochem Soc* 2017, **164**: A2298–A2303.

[89] Brogioli D, Langer F, Kun R, *et al*. Space-charge effects at the $Li_7La_3Zr_2O_{12}$/poly(ethylene oxide) interface. *ACS Appl Mater Interfaces* 2019, **11**: 11999–12007.

[90] Chinnam PR, Wunder SL. Engineered interfaces in hybrid ceramic–polymer electrolytes for use in all-solid-state Li batteries. *ACS Energy Lett* 2017, **2**: 134–138.

[91] Xu L, Tang S, Cheng Y, *et al*. Interfaces in solid-state lithium batteries. *Joule* 2018, **2**: 1991–2015.

[92] Chi S-S, Liu YC, Zhao N, *et al*. Solid polymer electrolyte soft interface layer with 3D lithium anode for all-solid-state lithium batteries. *Energy Storage Mater* 2019, **17**: 309–316.

[93] Shen B, Zhang T-W, Yin Y-C, *et al*. Chemically exfoliated boron nitride nanosheets form robust interfacial layers for stable solid-state Li metal batteries. *Chem Commun* 2019, **55**: 7703–7706.

[94] Huo HY, Chen Y, Luo J, *et al*. Rational design of hierarchical ceramic-in-polymer and polymer-in-ceramic electrolytes for dendrite-free solid-state batteries. *Adv Energy Mater* 2019, **9**: 1804004.

[95] Liang JN, Sun Q, Zhao Y, *et al*. Stabilization of all-solid-state Li–S batteries with a polymer–ceramic sandwich electrolyte by atomic layer deposition. *J Mater Chem A* 2018, **6**: 23712–23719.

[96] Stephan AM. Review on gel polymer electrolytes for lithium batteries. *Eur Polym J* 2006, **42**: 21–42.

[97] Zhang Z, Huang Y, Li C, *et al*. Metal–organic framework-supported poly(ethylene oxide) composite gel polymer electrolytes for high-performance lithium/sodium metal batteries. *ACS Appl Mater Interfaces* 2021, **13**: 37262–37272.

[98] Liu BY, Gong YH, Fu K, *et al*. Garnet solid electrolyte protected Li-metal batteries. *ACS Appl Mater Interfaces* 2017, **9**: 18809–18815.

[99] Zhang ZH, Zhao YR, Chen SJ, *et al*. An advanced construction strategy of all-solid-state lithium batteries with excellent interfacial compatibility and ultralong cycle life. *J Mater Chem A* 2017, **5**: 16984–16993.

[100] Zhou WD, Wang ZX, Pu Y, *et al*. Double-layer polymer electrolyte for high-voltage all-solid-state rechargeable batteries. *Adv Mater* 2019, **31**: 1805574.

[101] Liu Q, Zhou D, Shanmukaraj D, *et al*. Self-healing Janus interfaces for high-performance LAGP-based lithium metal batteries. *ACS Energy Lett* 2020, **5**: 1456–1464.

[102] Zhang NY, Wang GX, Feng M, *et al*. *In situ* generation of a soft–tough asymmetric composite electrolyte for dendrite-free lithium metal batteries. *J Mater Chem A* 2021, **9**: 4018–4025.

[103] Duan H, Yin Y-X, Shi Y, *et al*. Dendrite-free Li-metal battery enabled by a thin asymmetric solid electrolyte with engineered layers. *J Am Chem Soc* 2018, **140**: 82–85.

[104] Zhu P, Yan CY, Zhu JD, *et al*. Flexible electrolyte-cathode bilayer framework with stabilized interface for room-temperature all-solid-state lithium–sulfur batteries. *Energy Storage Mater* 2019, **17**: 220–225.

[105] Wan ZP, Lei DN, Yang W, *et al*. Low resistance—Integrated all-solid-state battery achieved by $Li_7La_3Zr_2O_{12}$ nanowire upgrading polyethylene oxide (PEO) composite electrolyte and PEO cathode binder. *Adv Funct Mater* 2019, **29**: 1805301.

[106] Duan H, Fan M, Chen W-P, *et al*. Extended electrochemical window of solid electrolytes via heterogeneous multilayered structure for high-voltage lithium metal batteries. *Adv Mater* 2019, **31**: 1807789.

[107] Judez X, Zhang H, Li CM, *et al*. Polymer-rich composite electrolytes for all-solid-state Li–S cells. *J Phys Chem Lett* 2017, **8**: 3473–3477.

[108] Dissanayake MAKL, Jayathilaka PARD, Bokalawala RSP, *et al*. Effect of concentration and grain size of alumina filler on the ionic conductivity enhancement of the $(PEO)_9LiCF_3SO_3$:Al_2O_3 composite polymer electrolyte. *J Power Sources* 2003, **119–121**: 409–414.

[109] Jayathilaka PARD, Dissanayake MAKL, Albinsson I, *et al*. Effect of nano-porous Al_2O_3 on thermal, dielectric and transport properties of the $(PEO)_9$LiTFSI polymer electrolyte system. *Electrochimica Acta* 2002, **47**: 3257–3268.

[110] Wang CH, Yang YF, Liu XJ, *et al*. Suppression of lithium dendrite formation by using LAGP–PEO (LiTFSI) composite solid electrolyte and lithium metal anode modified by PEO (LiTFSI) in all-solid-state lithium batteries. *ACS Appl Mater Interfaces* 2017, **9**: 13694–13702.

[111] Wu JY, Yuan LX, Zhang WX, *et al*. Reducing the thickness of solid-state electrolyte membranes for high-energy lithium batteries. *Energy Environ Sci* 2021, **14**: 12–36.

[112] Liu GZ, Shi JM, Zhu MT, *et al*. Ultra-thin free-standing sulfide solid electrolyte film for cell-level high energy density all-solid-state lithium batteries. *Energy Storage Mater* 2021, **38**: 249–254.

[113] Kim DH, Lee Y-H, Song YB, *et al*. Thin and flexible solid electrolyte membranes with ultrahigh thermal stability derived from solution-processable Li argyrodites for all-solid-state Li-ion batteries. *ACS Energy Lett* 2020, **5**: 718–727.

[114] Zhang ZH, Wu LP, Zhou D, *et al*. Flexible sulfide electrolyte thin membrane with ultrahigh ionic conductivity for all-solid-state lithium batteries. *Nano Lett* 2021, **21**: 5233–5239.

[115] Zha WP, Xu YH, Chen F, *et al*. Cathode/electrolyte interface engineering via wet coating and hot pressing for all-solid-state lithium battery. *Solid State Ion* 2019, **330**: 54–59.

[116] Chen R-J, Zhang Y-B, Liu T, *et al*. Addressing the interface issues in all-solid-state bulk-type lithium ion battery via an all-composite approach. *ACS Appl Mater Interfaces* 2017, **9**: 9654–9661.

[117] Fu XT, Yu DN, Zhou JW, *et al*. Inorganic and organic hybrid solid electrolytes for lithium-ion batteries. *CrystEngComm* 2016, **18**: 4236–4258.

[118] Srivastava S, Schaefer JL, Yang ZC, *et al*. 25th anniversary article: Polymer–particle composites: Phase stability and applications in electrochemical energy storage. *Adv Mater* 2014, **26**: 201–234.

[119] Zhang Z, Huang Y, Gao H, *et al*. MOF-derived multifunctional filler reinforced polymer electrolyte for solid-state lithium batteries. *J Energy Chem* 2021, **60**: 259–271.

[120] Choi J-H, Lee C-H, Yu J-H, *et al*. Enhancement of ionic conductivity of composite membranes for all-solid-state lithium rechargeable batteries incorporating tetragonal

$Li_7La_3Zr_2O_{12}$ into a polyethylene oxide matrix. *J Power Sources* 2015, **274**: 458–463.

[121] Yang LY, Wang ZJ, Feng YC, *et al*. Flexible composite solid electrolyte facilitating highly stable soft contacting Li–electrolyte interface for solid state lithium-ion batteries. *Adv Energy Mater* 2017, **7**: 1701437.

[122] Zhang YB, Chen RJ, Wang S, *et al*. Free-standing sulfide/polymer composite solid electrolyte membranes with high conductance for all-solid-state lithium batteries. *Energy Storage Mater* 2020, **25**: 145–153.

[123] Tu ZY, Kambe Y, Lu YY, *et al*. Nanoporous polymer–ceramic composite electrolytes for lithium metal batteries. *Adv Energy Mater* 2014, **4**: 1300654.

[124] Tang CY, Hackenberg K, Fu Q, *et al*. High ion conducting polymer nanocomposite electrolytes using hybrid nanofillers. *Nano Lett* 2012, **12**: 1152–1156.

[125] Zhang XK, Xie J, Shi FF, *et al*. Vertically aligned and continuous nanoscale ceramic–polymer interfaces in composite solid polymer electrolytes for enhanced ionic conductivity. *Nano Lett* 2018, **18**: 3829–3838.

[126] Lin DC, Liu W, Liu YY, *et al*. High ionic conductivity of composite solid polymer electrolyte via *in situ* synthesis of monodispersed SiO_2 nanospheres in poly(ethylene oxide). *Nano Lett* 2016, **16**: 459–465.

[127] Huang ZY, Pang WY, Liang P, *et al*. A dopamine modified $Li_{6.4}La_3Zr_{1.4}Ta_{0.6}O_{12}$/PEO solid-state electrolyte: Enhanced thermal and electrochemical properties. *J Mater Chem A* 2019, **7**: 16425–16436.

[128] Li WW, Sun CZ, Jin J, *et al*. Realization of the Li^+ domain diffusion effect via constructing molecular brushes on the LLZTO surface and its application in all-solid-state lithium batteries. *J Mater Chem A* 2019, **7**: 27304–27312.

[129] Zhang X, Liu T, Zhang SF, *et al*. Synergistic coupling between $Li_{6.75}La_3Zr_{1.75}Ta_{0.25}O_{12}$ and poly(vinylidene fluoride) induces high ionic conductivity, mechanical strength, and thermal stability of solid composite electrolytes. *J Am Chem Soc* 2017, **139**: 13779–13785.

[130] Zhang WQ, Nie JH, Li F, *et al*. A durable and safe solid-state lithium battery with a hybrid electrolyte membrane. *Nano Energy* 2018, **45**: 413–419.

[131] Liu H, He PG, Wang GX, *et al*. Thin, flexible sulfide-based electrolyte film and its interface engineering for high performance solid-state lithium metal batteries. *Chem Eng J* 2022, **430**: 132991.

[132] Ju JW, Wang YT, Chen BB, *et al*. Integrated interface strategy toward room temperature solid-state lithium batteries. *ACS Appl Mater Interfaces* 2018, **10**: 13588–13597.

[133] Zhang JJ, Zang X, Wen HJ, *et al*. High-voltage and free-standing poly(propylene carbonate)/$Li_{6.75}La_3Zr_{1.75}Ta_{0.25}O_{12}$ composite solid electrolyte for wide temperature range and flexible solid lithium ion battery. *J Mater Chem A* 2017, **5**: 4940–4948.

[134] Zheng J, Wang PB, Liu HY, *et al*. Interface-enabled ion conduction in $Li_{10}GeP_2S_{12}$–poly(ethylene oxide) hybrid electrolytes. *ACS Appl Energy Mater* 2019, **2**: 1452–1459.

[135] Hu CJ, Shen YB, Shen M, *et al*. Superionic conductors via bulk interfacial conduction. *J Am Chem Soc* 2020, **142**: 18035–18041.

[136] Bae J, Li YT, Zhang J, *et al*. A 3D nanostructured hydrogel-framework-derived high-performance composite polymer lithium-ion electrolyte. *Angew Chem Int Ed* 2018, **57**: 2096–2100.

[137] Liu W, Liu N, Sun J, *et al*. Ionic conductivity enhancement of polymer electrolytes with ceramic nanowire fillers. *Nano Lett* 2015, **15**: 2740–2745.

[138] Zhu P, Yan CY, Dirican M, *et al*. $Li_{0.33}La_{0.557}TiO_3$ ceramic nanofiber-enhanced polyethylene oxide-based composite polymer electrolytes for all-solid-state lithium batteries. *J Mater Chem A* 2018, **6**: 4279–4285.

[139] Sun JQ, Li YG, Zhang QH, *et al*. A highly ionic conductive poly(methyl methacrylate) composite electrolyte with garnet-typed $Li_{6.75}La_3Zr_{1.75}Nb_{0.25}O_{12}$ nanowires. *Chem Eng J* 2019, **375**: 121922.

[140] Zhai HW, Xu PY, Ning MQ, *et al*. A flexible solid composite electrolyte with vertically aligned and connected ion-conducting nanoparticles for lithium batteries. *Nano Lett* 2017, **17**: 3182–3187.

[141] Wang X, Zhai HW, Qie BY, *et al*. Rechargeable solid-state lithium metal batteries with vertically aligned ceramic nanoparticle/polymer composite electrolyte. *Nano Energy* 2019, **60**: 205–212.

[142] Liu XQ, Peng S, Gao SY, *et al*. Electric-field-directed parallel alignment architecting 3D lithium-ion pathways within solid composite electrolyte. *ACS Appl Mater Interfaces* 2018, **10**: 15691–15696.

[143] Song SF, Wu YM, Tang WP, *et al*. Composite solid polymer electrolyte with garnet nanosheets in poly(ethylene oxide). *ACS Sustain Chem Eng* 2019, **7**: 7163–7170.

[144] Hu LF, Tang ZL, Zhang ZT. New composite polymer electrolyte comprising mesoporous lithium aluminate nanosheets and PEO/$LiClO_4$. *J Power Sources* 2007, **166**: 226–232.

[145] Wang XZ, Zhang YB, Zhang X, *et al*. Lithium-salt-rich PEO/$Li_{0.3}La_{0.557}TiO_3$ interpenetrating composite electrolyte with three-dimensional ceramic nano-backbone for all-solid-state lithium-ion batteries. *ACS Appl Mater Interfaces* 2018, **10**: 24791–24798.

[146] Zhao Y, Yan JH, Cai WP, *et al*. Elastic and well-aligned ceramic LLZO nanofiber based electrolytes for solid-state lithium batteries. *Energy Storage Mater* 2019, **23**: 306–313.

[147] Li D, Chen L, Wang TS, *et al*. 3D fiber-network-reinforced bicontinuous composite solid electrolyte for dendrite-free lithium metal batteries. *ACS Appl Mater Interfaces* 2018, **10**: 7069–7078.

[148] Zhang Z, YingHuang, Zhang GZ, *et al*. Three-dimensional fiber network reinforced polymer electrolyte for dendrite-free all-solid-state lithium metal batteries. *Energy Storage Mater* 2021, **41**: 631–641.

[149] Yu SC, Xu Q, Lu X, *et al*. Single-ion-conducting "polymer-in-ceramic" hybrid electrolyte with an intertwined NASICON-type nanofiber skeleton. *ACS Appl Mater*

Interfaces 2021, **13**: 61067–61077.
[150] Wu H, Pan W, Lin DD, *et al*. Electrospinning of ceramic nanofibers: Fabrication, assembly and applications. *J Adv Ceram* 2012, **1**: 2–23.
[151] Bognitzki M, Czado W, Frese T, *et al*. Nanostructured fibers via electrospinning. *Adv Mater* 2001, **13**: 70–72.
[152] Fu SY, Zhu M, Zhu YF. Organosilicon polymer-derived ceramics: An overview. *J Adv Ceram* 2019, **8**: 457–478.
[153] Xie H, Yang CP, Fu K, *et al*. Flexible, scalable, and highly conductive garnet-polymer solid electrolyte templated by bacterial cellulose. *Adv Energy Mater* 2018, **8**: 1703474.
[154] Gong YH, Fu K, Xu SM, *et al*. Lithium-ion conductive ceramic textile: A new architecture for flexible solid-state lithium metal batteries. *Mater Today* 2018, **21**: 594–601.
[155] Dai JQ, Fu K, Gong YH, *et al*. Flexible solid-state electrolyte with aligned nanostructures derived from wood. *ACS Mater Lett* 2019, **1**: 354–361.
[156] Bae J, Li YT, Zhao F, *et al*. Designing 3D nanostructured garnet frameworks for enhancing ionic conductivity and flexibility in composite polymer electrolytes for lithium batteries. *Energy Storage Mater* 2018, **15**: 46–52.
[157] Jiang TL, He PG, Wang GX, *et al*. Solvent-free synthesis of thin, flexible, nonflammable garnet-based composite solid electrolyte for all-solid-state lithium batteries. *Adv Energy Mater* 2020, **10**: 1903376.
[158] Information on https://www.academia.edu/41997371/Could_3D_Printing_Change_the_World_Technologies_Potential_and_Implications_of_Additive_Manufacturing.
[159] Chen Z, Sun XH, Shang YP, *et al*. Dense ceramics with complex shape fabricated by 3D printing: A review. *J Adv Ceram* 2021, **10**: 195–218.
[160] Hassanin H, Essa K, Elshaer A, *et al*. Micro-fabrication of ceramics: Additive manufacturing and conventional technologies. *J Adv Ceram* 2021, **10**: 1–27.